

We are IntechOpen, the world's leading publisher of Open Access books Built by scientists, for scientists

6,900

Open access books available

185,000

International authors and editors

200M

Downloads

Our authors are among the

154

Countries delivered to

TOP 1%

most cited scientists

12.2%

Contributors from top 500 universities



WEB OF SCIENCE™

Selection of our books indexed in the Book Citation Index
in Web of Science™ Core Collection (BKCI)

Interested in publishing with us?
Contact book.department@intechopen.com

Numbers displayed above are based on latest data collected.
For more information visit www.intechopen.com



Bioactive Microarc Oxidized TiO₂-based Coatings for Biomedical Implication

Daqing Wei and Yu Zhou
Harbin Institute of Technology
China

1. Introduction

Hydroxyapatite ($\text{Ca}_{10}(\text{PO}_4)_6(\text{OH})_2$, HA) and bioactive glass-ceramic ($\text{SiO}_2\text{-CaO-P}_2\text{O}_5\text{-MO}$ (M=Na, Mg, etc.)) both exhibit good bioactivity. Unfortunately, these bioactive ceramic materials are not suitable for load-bearing conditions on account of their poor mechanical properties (Liu et al., 2004; Morais et al., 2007). As compared to these brittle ceramics, metal materials such as titanium and its alloys exhibit excellent mechanical toughness and strength (Liu et al., 2004). However, they have poor osteoinductive properties because of their bioinert feature. Thus, to prepare bioactive coatings on titanium and its alloys is an approach to resolving the disadvantages of ceramic and metal biomaterials. Many surface modifying techniques (e.g., plasma spraying (Zheng et al., 2000), sol-gel method (Wen et al., 2007; Balamurugan et al., 2007), biomimetic and electrochemical deposition (Zhang et al., 2005)) have been developed to deposit bioactive coating on titanium and its alloys.

Microarc oxidation (MAO) is a relatively convenient and effective technique to deposit bioceramic coatings on the surfaces of Ti and its alloys (Yerokhin et al., 1999). This technique can introduce various desired elements into titania-based coatings and produce various functional coatings with a porous structure (Yerokhin et al., 1999). Additionally, MAO coatings usually exhibit good interfacial bonding to substrates (Wang et al., 2009). Moreover, it is very suitable to modify various substrates with complex geometries. Most of MAO coatings mainly contained anatase, rutile and amorphous or crystalline calcium phosphate phase (at high applied voltage). It is difficult to form HA phase during MAO process because of a high temperature and a rapid cooling rate at anodic surfaces. And the apatite-forming ability of the MAO coatings is not very good. Thus, the subsequent modifications have been developed such as sol-gel, ultraviolet (UV) irradiation and hydrothermal treatment (Li et al., 2005; Han et al., 2008; Ishizawa et al., 1995). Authors have developed a simple method of chemical-treatment to modify the surfaces of the MAO coatings for improving the induction ability for the formation of biomimetic apatite (Wei^a et al., 2007; Wei et al., 2008).

In addition, the formation process of biomimetic apatite on the bioactive surface has been noted for long time. However, some important problems were also not solved until now. Thus, systematic thermodynamic and kinetic calculations of Gibbs free energy (ΔG) and nucleation rate ($\log J$) for the formation of various calcium phosphates (CaPs) in different simulated body fluids (SBFs) was conducted by authors. The structure and formation process of biomimetic apatite were reported.

2. Formation bioactive MAO coatings on titanium and its alloys for inducing biomimetic apatite

Using MAO technique to deposit bioactive ceramic coatings on titanium and its alloys has received much attention in recent years (Fini et al., 1999; Zhu et al., 2001; Zhu et al., 2002; Zhu et al., 2002; Han et al., 2003; Frauchiger et al., 2004; Li et al., 2004; Song et al., 2004; Li et al., 2005; Zhang et al., 2004; Rodriguez et al., 2003). To prepare the bioactive coatings on titanium and its alloys, introductions of Ca and P elements into MAO were taken into account. In previous studies, various calcium salts such as calcium acetate, β -glycerophosphate disodium salt pentahydrate, calcium glycerophosphate and calcium dihydrogen phosphate were used in MAO process.

In the previous research, titania-based coatings on titanium were prepared by MAO at various applied voltages (250-500V) in an electrolytic solution containing β -glycerophosphate disodium salt pentahydrate and calcium acetate monohydrate (Song et al., 2004). Ca- and P-containing titania-based coatings were formed on the titanium substrates. The phase, Ca and P content, morphology and thickness of the coatings were strongly dependent on the applied voltage. In particular, Ca- and P-containing compounds such as CaTiO_3 , $\text{Ca}_2\text{P}_2\text{O}_7$ and $\text{Ca}_3(\text{PO}_4)_2$ were produced at higher voltages (>450 V). Besides the β -glycerophosphate disodium salt pentahydrate, calcium glycerophosphate was also used. In the electrolyte of calcium glycerophosphate and calcium acetate, the titanium anodic oxide coating is porous, highly crystalline, and rich in Ca and P. The optimum condition is that the concentration of the electrolyte is 0.02M calcium glycerophosphate and 0.15M calcium acetate, and current density and final voltage are 70 A/m² and 350 V, respectively (Zhu et al., 2001). To achieve high amounts of Ca, researchers (Frauchiger et al., 2004) used a new electrolyte containing Ca-EDTA chelate complex to prepare MAO coating. Based on the previous researches, authors have developed the MAO coatings only containing P. The MAO coating formed at 300 and 350 V after oxidizing for 5 min show good surface properties.

In addition, as mentioned above, to achieve high amounts of Ca, EDTA was used to add into the electrolyte. Authors further investigated the effects of applied voltage and electrolyte composition and concentrations on the structures of the MAO coatings (e.g., phase composition, surface morphology, micropore number and size, element distribution on the surface and cross-sectional characters, etc) (Wei^b et al., 2007). In the MAO coating formed on Ti6Al4V, TiO_2 nanocrystals were randomly distributed in Ca- and P-doped matrix, and their crystal size was 30-40 nm. With increasing the applied voltage, the surface toughness, micropores size, Ca and P concentrations, coating thickness are increased. High applied voltage promoted the formation of rutile. However, besides the TiO_2 and amorphous phase were observed, no other phase were detected at different applied voltages, not similar the previous researches. In this electrolyte, the EDTA impeded the crystallization of TiO_2 crystals during the MAO process. Besides the above electrolyte, the similar electrolyte with addition of HA was also investigated. It was found that the addition of HA promoted the formation of anatase (Wei^c et al., 2007).

Recently, bioactive glass components (BGC) doped MAO coatings on titanium were noticed by authors. This electrolyte was composed of $\text{Ca}(\text{CH}_3\text{COO})_2 \cdot \text{H}_2\text{O}$, Na_2SiO_3 , EDTA-2Na and NaOH. And the results indicated that the surface morphology, phase composition and elemental concentrations are highly depended on the applied voltages. And BGC doped TiO_2 -based coatings exhibit good interface bonding with titanium, showing a graded

structure in elemental concentrations of Si, Ca, Na, O, Ti, etc.. Moreover, these elements were distributed uniformly on the surface of BGC doped TiO₂-based coatings. During the MAO treatment process, Ti could not be oxidized sufficiently, thus the TiO phase was also formed according to XPS results.

Based on the above researches, generally speaking, the structures such as phase composition, surface morphology and elemental composition of the MAO coatings are highly dependent on the MAO process parameters such as the applied voltage, oxidizing time, frequency, duty cycle and electrolyte composition, etc., especially the applied voltage and electrolyte composition.

3. The improvement of bioactivity of MAO coatings by surface modifications

Most of MAO coatings mainly contain anatase, rutile and amorphous or crystalline calcium titanate and calcium phosphate phase, etc. (at high applied voltage). It is difficult to form HA phase during MAO process because of a high temperature and a rapid cooling rate at anodic surfaces. In fact, MAO coating may possess specific surface structures such as amorphous phase, nonequilibrium solid, complex mixed-compounds, etc, since complex plasma physical and chemical reactions such as ionization and plasma condensation, etc occur at electrode surfaces. Based on the previous researches (Han et al., 2008), the apatite-forming ability and bioactivity of most of MAO coatings are not very good. Thus, subsequent activation methods such as sol-gel, ultraviolet (UV) irradiation and hydrothermal treatments have been investigated to improve the surface bioactivity of MAO coatings, as mentioned above.

In the previous research (Song et al., 2004; Han et al., 2003), the MAO coating containing Ca and P formed at higher voltages (>450 V) was immersed in a simulated body fluid for 28 days, a carbonated hydroxyapatite was induced on the surfaces. This MAO coating contained CaTiO₃, Ca₂P₂O₇ and Ca₃(PO₄)₂, which play key roles for the formation of the biomimetic apatite (Han et al., 2003).

Researchers have sought the methods to improve the ability of the MAO coatings to induce the formation of biomimetic apatite. The hydrothermal treatment is the common method to change the surface structure of the MAO coatings to formation of hydroxyapatite/titania composite coatings. Regarding to the hydrothermal treatment of the MAO coatings, researches have been extensively reported in the past. As reported, a MAO coating containing Ca and P was formed on commercially pure titanium which was anodized in an electrolytic solution of dissolved β -glycerophosphate and calcium acetate. HA crystals were precipitated by hydrothermally treating the MAO coating at 300°C. The morphology, composition, and amount of HA crystals were significantly dependent on the electrolytes composition (Ishizawa et al., 1995).

In the previous research (Huang et al. 2004), surface modification of titanium implant is processed by microarc oxidation and hydrothermal treatment. A porous surface with a biologically active bone-like apatite layer was formed. The apatite layer consists of very fine crystals and high crystallinity and is integrated with the titanium alloy substrate with a graded structure without a distinct interface. Such a bioactive layer is expected not only to enhance the bone ingrowth into the porous structure, but also to improve the interlocking between implant and bone.

The Ca-doped MAO coating without addition of P was also investigated (Song et al., 2005). This MAO coating showed no apatite-formation during the testing process. However, after a

hydrothermal treatment at 250°C, apatite was formed on the surfaces of the CaTiO₃-embedded titania after 28 days, which was closely related to the formation of amorphous Ca(OH)₂ and presumably surface Ti-OH groups.

The other treatment method is using UV irradiation to modify MAO titania coating. Based on the previous researches (Han et al., 2008), an enhanced bioactivity and cell response to titania after UV irradiation was achieved. Compared to the MAO coating, the UV-irradiated MAO coatings do not exhibit any obvious change in surface roughness, morphology, grain size and phase component; however, they have more abundant basic Ti-OH groups and become more hydrophilic because the water contact angle decreases significantly. In SBF, bonelike apatite-forming ability is significantly stronger on the UV-irradiated coatings than the MAO coating.

Sol-gel was also used to change the bioactivity of the MAO coatings. Thin HA layers could be deposited on MAO coatings by sol-gel method (Li et al., 2005). The bioactivity of the MAO coating was improved further by the sol-gel HA coating on the MAO treated Ti. The porous morphology and roughness of the MAO coatings was changed slightly after sol-gel treatment.

Based on the above researches, authors have developed a simple chemical-treatment to modify the surface of the MAO coatings (Wei^a et al., 2007; Wei et al., 2008). In this process, the MAO coatings were treated by NaOH aqueous solution with different concentrations. After alkali-treatment, the surfaces of the MAO coatings containing Ca and P become rough, and the Ca and P concentrations decrease with increasing the concentration of NaOH solution. When 5 mol/L NaOH solution was used, amorphous calcium titanate hydrogel was formed on the surface, showing a nanoflake-like morphology with an approximately oriented structure. During the alkali-treatment process, Ca and P on the surface of the MAO coating show a process of dissolution. At the same time, negatively charged HTiO₃⁻ ions are formed on the MAO coating surface due to the attack of OH⁻ on the TiO₂ phase of the MAO coating. Then, the negatively charged ions could incorporate sodium from the alkali solution and calcium from the alkali solution and MAO coating to form the titanates hydrogels.

In the case of MAO coatings containing P after alkali-treatment (Wei et al., 2008), ribbon-like products with an interlaced morphology were found on the surface. During the chemical etching process, P of the surface of the MAO coating dissolved into the NaOH aqueous solution. Negatively charged HTiO₃⁻ ions are formed on the MAO coating surface due to the attack of OH⁻ ions on TiO₂ phase of the MAO coating. The negatively charged HTiO₃⁻ ions could incorporate sodium ions from the NaOH aqueous solution to form sodium titanate.

4. Structure and formation of biomimetic apatite on the surface of chemical-treated MAO coatings

4.1 The composition of biomimetic apatite

Apatites have been used in medicine and dentistry for long time. The interest in one group member, HA, arises from its similarity to bone apatite, the major component of the inorganic phase of bone, which plays a key role in the calcification and resorption processes of bone. Different phases of calcium phosphate ceramics such as HA and Ca₃(PO₄)₂ (TCP) can be used in medicine, depending on whether a bioactive or a resorbable material is desired. Apatite is the name given to a group of crystals of the general chemical formula M₁₀(RO₄)X₂, where R is most commonly phosphorus, M could be one of several metals, although it

usually calcium, and X is commonly hydroxide or a halogen such as fluorine or chlorine. Hydroxyapatite belongs to the apatite family, which is the most commonly used calcium phosphate in the medical field, as it possesses excellent biocompatibility and is osteoconductive.

The apatite structure is very hospitable in allowing the substitutions of many other ions, which makes people to bethink of biological apatites. The biological apatites constitute the mineral phase of calcified tissues such as bone, dentine and enamel in the body. They are similar to synthetic HA, but they differ from HA in composition, stoichiometry, and physical and mechanical properties. Biological apatites are usually calcium-deficient as a result of various substitutions at regular HA lattice points. The general chemical formula for biological apatites is $(\text{Ca}, \text{M})_{10}(\text{PO}_4, \text{CO}_3, \text{Y})_6(\text{OH}, \text{F}, \text{Cl})_2$. Where M represents metallic elements such as Na, K, and Mg, and Y represents functional groups such as acid phosphate, sulfates, etc..

As well known, the bones and teeth of all vertebrates are natural composite materials, where one of the components is an inorganic solid, carbonate hydroxyapatite. Thus, the formation of the carbonate hydroxyapatite in vitro by biomimetic method is worthy to be noticed. According to the previous researches [Müller et al., 2006; Wei^a et al., 2007; Wei et al., 2008], the biomimetic apatites of A-type slightly substituted carbonated-HA (SCHA-A) and B-type slightly substituted carbonated-HA with HPO_4^{2-} group (HPO4-SCHA-B) have been reported extensively. At the same time, Na, K, Mg and Cl elements could be also introduced into these apatites, however, the concentrations of these elements are very small. In addition, it is interesting that the induced biomimetic apatite presented two-level porous structure on micro- and nano-scales, which has less been reported according to authors' studies [Wei et al., 2009].

4.2 The formation of Ti-OH group and its induction for biomimetic apatites

During the SBF immersion process, a variety of reactions such as dissolution, ion exchange and precipitation occur on the surface of the chemical-treated MAO coatings. The Ca could release from the surface of the MAO coating. An ionic exchange between Ca^{2+} of the chemical-treated MAO coatings and H_3O^+ of the SBF takes place during SBF immersion process. As a result, abundant Ti-OH groups are formed on the surface of the chemical-treated MAO coating. Also, the Na^+ ions on the chemical-treated MAO coating could participate in the ionic exchange process, promoting the formation of Ti-OH groups.

Generally, substrates with functionalized surfaces such as -OH, PO_4H_2 , COOH , SO_3H , and CONH_2 groups facilitate the formation of bonelike apatite in SBF or solutions containing various ions with respect to apatite [Toworfe et al., 2006; Liu et al., 2002].

The nucleation and growth of biomimetic apatite generate from an interfacial molecular recognition between functionalized surface and ions with respect to apatite in solutions. The interfacial molecular recognition involves certain aspects such as electrostatic potential interaction [Toworfe et al., 2006]. According to the previous researches [Wei^a et al., 2007; Wei et al., 2008; Toworfe et al., 2006], the electrostatic potential interaction is that the Ti-OH groups incorporate calcium ions, and then absorb the phosphate and carbonic acid ions in the SBF. The absorbed negative ions such as phosphate and carbonic acid ions could further attract the calcium ions etc.. With increasing the immersion time, the supersaturation degree of solution with respect to apatite near the vicinity of the Ti-OH group occurs, which triggers the apatite nucleation. Once the apatite nuclei are formed, they grow spontaneously by assembling the remaining calcium, phosphate and carbonic acid ions around apatite nuclei in the SBF.

5. Theoretical calculation and understanding the mechanism of biomimetic apatite formation in SBF on the surfaces of bioactive coatings

In order to understand the formation of various calcium phosphates (CaPs) thoroughly, theoretical calculations were conducted by many researchers. In the previous results, thermodynamic analyses of CaPs have been reported in the solutions including $\text{CaCl}_2+\text{NaCl}+\text{NaH}_2\text{PO}_4+\text{NaOH}$ [Boistelle et al., 1990], HA powder+ $\text{HCl}+\text{KOH}+\text{NaCl}$ [Feng et al., 2000], $\text{NaCl}+\text{CaCl}_2+\text{KH}_2\text{PO}_4$ [Wu et al., 1997] $\text{CaCl}_2+\text{KH}_2\text{PO}_4+\text{KOH}$ [Koutsoukos et al., 1980; Koutsoukos et al., 1981], $\text{Ca}(\text{NO}_3)_2+\text{KH}_2\text{PO}_4+\text{NaOH}$ [^aHeughebaert et al., 1984; ^bHeughebaert et al., 1984], $\text{CaCl}_2+\text{KH}_2\text{PO}_4+\text{NaCl}+\text{KOH}$ [Koutsopoulos et al., 1994; Koutsopoulos et al., 2000;]. In fact, understanding the formation of CaPs in SBF is very important and valuable, since SBFs were widely used to obtain biomimetic apatite or evaluate the apatite-inducing ability of biomaterials. Thus, the thermodynamics and kinetics for the fomation of various CaPs in SBF are necessary. Based on this purpose, researchers [Boistelle, et al., 1990; Lu et al., 2005] have conducted the thermodynamic and kinetics of $\text{Ca}_4(\text{HPO}_4)(\text{PO}_4)_2$ (OCP), CaHPO_4 (DCPD) and HA, etc.. Besides OCP, DCPD and HA, researches indicated that biomimetic apatites such as carbonated HA containing HPO_4^{2-} group were formed on the samples after SBF immersion [Müller et al., 2006; Wei^a et al., 2007; Wei et al., 2008;]. In addition, the relationships among the ions concentration, supersaturation, Gibbs free energy, critical nucleation are not very clear. We feel that there lacks an overall and systematic thermodynamic and kinetic guidelines for various CaPs such as DCPD, OCP, $\text{Ca}_3(\text{PO}_4)_2$ (TCP), HA, $\text{Ca}_9(\text{HPO}_4)(\text{PO}_4)_5\text{OH}$ (DOHA), A-type slightly substituted carbonated-HA (SCHA-A) and B-type slightly substituted carbonated-HA with HPO_4^{2-} group (HPO4-SCHA-B), etc. formation in SBF. In this work, authors calculated the thermodynamic and kinetic processes of common CaPs mentioned above. According to the calculated results, the apatites induced by bioactive coatings were explained.

5.1 Analytical model

In this work, various SBFs with different ion concentrations were considered as shown in Table 1, because the composition, concentration, pH, etc. of the SBFs could affect the phase composition, crystallinity and crystal growth rate of biomimetic apatites. In the text, if no other explanation, the used SBF for calculation is referred to the c-SBF.

Blood plasma and SBF	Ion concentration (mmol/L)							
	Na ⁺	K ⁺	Mg ²⁺	Ca ²⁺	Cl ⁻	HCO ³⁻	HPO ⁴ 2 ⁻	SO ⁴ 2 ⁻
Blood plasma	142.0	5.0	1.5	2.5	103.0	27.0	1.0	0.5
c-SBF	142.0	5.0	1.5	2.5	147.8	4.2	1.0	0.5
r-SBF	142.0	5.0	1.5	2.5	103.0	27.0	1.0	0.5
i-SBF	142.0	5.0	1.0	1.6	103.0	27.0	1.0	0.5
m-SBF	142.0	5.0	1.5	2.5	103.0	10.0	1.0	0.5
HBSS	142	5.81	126	0.898	146	4.17	0.779	0.406

Table 1. Composition of different SBFs and blood plasma

If the supersaturation regarding to apatites of the SBFs is high enough, the formation of the apatites in the SBFs is possible on thermodynamically. The classical equation of Gibbs free energy change in supersaturated sultions was shown below [Mullin et al., 2001]:

$$\Delta G = -\frac{RT}{n}\ln(S) = -\frac{RT}{n}\ln\left(\frac{A_p}{K_{sp}}\right) \tag{1}$$

where ΔG is the Gibbs free energy per mole of ionic units that compose CaPs in solution, R is the gas constant ($8.314\text{ JK}^{-1}\text{ mol}^{-1}$), n is the number of ion units in a CaPs molecule, T is the absolute temperature and S is the supersaturation that is defined by the ratio of the activity product of ion units composing precipitates (A_p) to the corresponding solubility product (K_{sp}).

In this work, the ΔG for the formation of the CaPs including DCPD, OCP, DOHA, TCP, HA, SCH A-A-0.5, SCH A-A-1, SCH A-B-1 and HPO4-SCH A-B-0.5 were investigated, as shown in Table 2.

Calcium phosphates	Reactions	Ksp	Reference	Equ.
DCPD	$\text{Ca}^{2+}+\text{HPO}_4^{2-}=\text{CaHPO}_4$	$10^{-6.622}$	[Lu et al., 2005]	(2)
OCP	$4\text{Ca}^{2+}+\text{HPO}_4^{2-}+2\text{PO}_4^{3-}=\text{Ca}_4(\text{HPO}_4)(\text{PO}_4)_2$	$10^{-36.48}$	[Lu et al., 2005]	(3)
DOHA	$9\text{Ca}^{2+}+5\text{PO}_4^{3-}+\text{HPO}_4^{2-}+\text{OH}^- =\text{Ca}_9(\text{HPO}_4)(\text{PO}_4)_5\text{OH}$	$10^{-85.1}$	[Lu et al., 2005]	(4)
TCP	$3\text{Ca}^{2+}+2\text{PO}_4^{3-}=\text{Ca}_3(\text{PO}_4)_2$	$10^{-117.2}$	[Müller et al., 2006]	(5)
HA	$10\text{Ca}^{2+}+6\text{PO}_4^{3-}+2\text{OH}^-=\text{Ca}_{10}(\text{PO}_4)_6(\text{OH})_2$	2.83×10^{-30}	[Koutsopoulos et al., 2000]	(6)
SCH A-A-0.5	$10\text{Ca}^{2+}+6\text{PO}_4^{3-}+1/2\text{CO}_3^{2-}+\text{OH}^- =\text{Ca}_{10}(\text{PO}_4)_6(\text{OH})(\text{CO}_3)_{0.5}$	$10^{-115.6}$	[Lu et al., 2005]	(7)
SCH A-A-1	$10\text{Ca}^{2+}+6\text{PO}_4^{3-}+\text{CO}_3^{2-}=\text{Ca}_{10}(\text{PO}_4)_6\text{CO}_3$	10^{-85}	[Ito et al., 1997]	(8)
SCH A-B-1	$9\text{Ca}^{2+}+5\text{PO}_4^{3-}+\text{CO}_3^{2-}+\text{OH}^- =\text{Ca}_9(\text{PO}_4)_5(\text{CO}_3)(\text{OH})$	$10^{-73.7}$	[Ito et al., 1997]	(9)
HPO4-SCH A-B-0.5	$9\text{Ca}^{2+}+1/2\text{HPO}_4^{2-}+5\text{PO}_4^{3-}+1/2\text{CO}_3^{2-}+\text{OH}^-=\text{Ca}_9(\text{HPO}_4)_{0.5}(\text{PO}_4)_5(\text{CO}_3)_{0.5}(\text{OH})$	$10^{-115.4}$	[Lu et al., 2005; Koutsopoulos et al., 2000]	(10)

Table 2. Kinds of calcium phosphates and their synthesized reactions

For examples, the supersaturation S of OCP and SCH A-A-0.5 were calculated by the following equations:

$$S(\text{OCP}) = \frac{(\gamma_{\text{Ca}^{2+}})^4(\gamma_{\text{HPO}_4^{2-}})(\gamma_{\text{PO}_4^{3-}})^2[\text{Ca}^{2+}]^4[\text{HPO}_4^{2-}][\text{PO}_4^{3-}]^2}{K_{\text{SP}}(\text{OCP})} \tag{11}$$

$$S(\text{SCH A-A-0.5}) = \frac{(\gamma_{\text{Ca}^{2+}})^{10}(\gamma_{\text{PO}_4^{3-}})^6(\gamma_{\text{CO}_3^{2-}})^{0.5}(\gamma_{\text{OH}^-})[\text{Ca}^{2+}]^{10}[\text{PO}_4^{3-}]^6[\text{CO}_3^{2-}]^{0.5}[\text{OH}^-]}{K_{\text{SP}}(\text{SCH A-A-0.5})} \tag{12}$$

The S of the other CaPs could be calculated by similar method.

In these equations, $[\text{Ca}^{2+}]$, $[\text{PO}_4^{3-}]$, $[\text{CO}_3^{2-}]$, $[\text{OH}^-]$ and $[\text{HPO}_4^{2-}]$ are the equilibrium concentrations of the corresponding ions in the SBF. The $\gamma_{\text{Ca}^{2+}}$, $\gamma_{\text{PO}_4^{3-}}$, $\gamma_{\text{CO}_3^{2-}}$, γ_{OH^-} and $\gamma_{\text{HPO}_4^{2-}}$ are the activity coefficients of the corresponding ions in the SBF. In order to obtain the equilibrium concentrations, the possible chemical association/dissociation reactions

regarding to CaPs were should be taken into account firstly as shown in Table 3 [Oyane, et al., 2003].

Chemical reaction	K
$H_2CO_3(aq.) \leftrightarrow H^+ + HCO_3^-$	$10^{-6.31}$
$HCO_3^- \leftrightarrow H^+ + CO_3^{2-}$	$10^{-10.25}$
$HPO_4(aq.) \leftrightarrow H^+ + H_2PO_4^-$	$10^{-2.196}$
$H_2PO_4^- \leftrightarrow H^+ + HPO_4^{2-}$	$10^{-7.185}$
$HPO_4^{2-} \leftrightarrow H^+ + PO_4^{3-}$	$10^{-12.19}$
$Ca^{2+} + HCO_3^- \leftrightarrow CaHCO_3^+$	$10^{1.16}$
$Ca^{2+} + CO_3^{2-} \leftrightarrow CaCO_3(aq.)$	$10^{3.38}$
$Ca^{2+} + OH^- \leftrightarrow CaOH^+$	25.12
$Ca^{2+} + H_2PO_4^- \leftrightarrow CaH_2PO_4^+$	31.9
$Ca^{2+} + HPO_4^{2-} \leftrightarrow CaHPO_4(aq.)$	6.81×10^2
$Ca^{2+} + PO_4^{3-} \leftrightarrow CaPO_4^-$	3.46×10^6

Table 3. The possible chemical association/dissociation reactions in SBF [Oyane, et al., 2003]
Based on these association/dissociation reactions, three mass balance equations are used to calculate the ions equilibrium concentration in SBF:

$C_{Ca^{2+}}=[Ca^{2+}]+[CaOH^+]+[CaCO_3]+[CaH_2PO_4^+]+[CaHPO_4]+[CaPO_4^-]+[CaHCO_3^+]$ (13)

$C_{HCO_3^-}=[HCO_3^-]+[CO_3^{2-}]+[H_2CO_3]+[CaHCO_3^+]+[CaCO_3]$ (14)

$C_{HPO_4^{2-}}=[HPO_4^{2-}]+[HPO_4^-]+[PO_4^{3-}]+[CaH_2PO_4^+]+[CaHPO_4]+[H_2PO_4^-]+[CaPO_4^-]$ (15)

Where the $C_{Ca^{2+}}$, $C_{HCO_3^-}$ and $C_{HPO_4^{2-}}$ is the initial addition concentration shown in Table 1 and the [] is the equilibrium concentration.
According to the equation of Debye-Hückel, the γ_i can be calculated by the following equations [Mullin et al., 2001]:

$$\lg \gamma_i = -Az_i^2[\frac{I^{1/2}}{1+I^{1/2}} - 0.3I]$$
 (16)

$$I = \frac{1}{2} \sum_i c_i z_i^2$$
 (17)

where A is the Debye-Hückel constant dependent on temperature $A=0.5211(37^{\circ}C)$, I is the total ionic strength of the SBF, z_i is the charge number of ions and c_i is the molar concentration of each ion unit.
According to the previous results [Weia et al., 2007; Wei et al., 2008], the apatite formation on the surface of the bioactive coatings is a heterogeneous nucleation process. And the heterogeneous nucleation energy (ΔG_{het}) is calculated by the following equation [Mullin et al., 2001]:

$$\Delta G_{het} = \frac{16\pi\sigma^3 v^2 f(\theta)}{3(kT \ln S)^2}$$
 (18)

Where σ is the surface energy of per unit area (surface tension), v is the molecule volume of crystal, k is the Boltzmann constant and T is the absolute temperature, the $f(\theta)$ is a function of contacting angle, θ , between crystal body and substrate, and was calculated by the following equation [Mullin et al., 2001]:

$$f(\theta) = \left(\frac{(2 + \cos \theta)(1 - \cos \theta)^2}{4} \right) \quad (19)$$

In the Equ. 19, the $\cos \theta$ was calculated by the following equation [Mullin et al., 2001]:

$$\cos \theta = \frac{\sigma_{L\beta} - \sigma_{\alpha\beta}}{\sigma_{\alpha L}} \quad (20)$$

where $\sigma_{L\beta}$ is the interface tension between liquid phase and substrate, $\sigma_{\alpha\beta}$ is the interface tension between nuclear and substrate and $\sigma_{\alpha L}$ is the interface tension between liquid phase and nuclear. In this work, the θ was assumed as 90° based on the previous researches [Wei^a et al., 2007; Wei et al., 2008; Lu et al., 2005].

In this work, the critical nucleus, r_c , of various CaPs were calculated by the following equation [25]:

$$r_c = \frac{2\sigma v}{kT \ln S} \quad (21)$$

Based on the above data, the nucleation rates of various CaPs were calculated by the following equation [Mullin et al., 2001]:

$$J = K \cdot \exp\left(-\frac{\Delta G}{kT}\right) = K \cdot \exp\left(-\frac{16\pi v^2 \sigma^3 f(\theta)}{3k^3 T^3 (\ln S)^2}\right) \quad (22)$$

In this equation, K is a kinetic factor, which is independent of the substrates and not a constant. For different chemical reactions, the K value is different. Boistelle et al. [Boistelle, et al., 1990] proposed a mathematics mode to calculate the K , as shown in the following equation:

$$K = K'P \quad (23)$$

where K' is a constant ($13.64 \times 10^{-24} \text{cm}^3 \text{s}^{-1}$) and P is nucleation probability. When the molecular formula of CaP is $A_1(n_1)A_2(n_2)\dots A_i(n_i)$ (where A_i is atom species/molecule and n_i is the amount of the A_i atom/molecule), P was calculated by the following equation [Boistelle, et al., 1990]:

$$P = \frac{(n_1 + n_2 + \dots + n_i)! \times [A_1^{z_1}]^{n_1} [A_2^{z_2}]^{n_2} \dots [A_i^{z_i}]^{n_i}}{n_1! n_2! \dots n_i! \times \{[A_1^{z_1}] + [A_2^{z_2}] + \dots + [A_i^{z_i}]\}^{(n_1 + n_2 + \dots + n_i)}} \quad (24)$$

Where, the $[A_i^{z_i}]$ denoted the ion concentration corresponding to the A_i atom/molecule. For example, P of the HPO₄-SCHA-B-0.5 was calculated by the following Equ. 25:

$$P = \frac{(9 + 0.5 + 5 + 0.5 + 1)! \times [\text{Ca}^{2+}]^9 [\text{HPO}_4^{2-}]^{0.5} [\text{PO}_4^{3-}]^5 [\text{CO}_3^{2-}]^{0.5} [\text{OH}]^1}{9!0.5!5!0.5!1! \times \left\{ [\text{Ca}^{2+}] + [\text{HPO}_4^{2-}] + [\text{PO}_4^{3-}] + [\text{CO}_3^{2-}] + [\text{OH}] \right\}^{(9+0.5+5+0.5+1)}} \quad (25)$$

Boistelle et al. used this equation to calculate the P of DCPD, OCP and HA [Boistelle, et al., 1990]. Leng et al. [Lu et al., 2005] used this mode to further calculate the P of DOHA and SCHA-A-0.5. In this work, the P of TCP, SCHA-A-1, SCHA-B-1 and HPO4-SCHA-B-0.5 were calculated by this equation.

In the previous researches [Lu et al., 2005], the measurements could affect the value of σ of the apatite. Even different researchers provided different σ values using same measurement [Lu et al., 2005]. Thus, it brought out the difficulty to obtain the accurate value of σ . In addition, there has no available data for SCHA-A-0.5 and HPO4-SCHA-B-0.5 et al.. Thus it was considered to obtain the σ value by theoretical calculation.

In 1990s, Mersmann et al. [Mullin et al., 2001] proposed an equation to calculate the σ value:

$$\sigma = 0.414kT \left[\frac{\rho_c N}{M} \right]^{2/3} \ln \left[\frac{c_s}{c_L} \right] \quad (26)$$

where k is boltzmann constant ($1.38 \times 10^{-23} \text{J K}^{-1}$), N is Avogadro constant ($6.02 \times 10^{26} \text{kmol}^{-1}$), M is molar mass (kg kmol^{-1}), ρ_c is the crystal density (kg m^{-3}), c_s and c_L are the solute concentrations (kmol m^{-3}) in the solid and liquid phases.

In order to calculate conveniently, the above equation was deduced further. The following two equations were introduced into the Equ.26.

$$\rho_c = \frac{M}{N \cdot v} \quad (27)$$

$$c_s = \frac{\rho_c}{M} = \frac{1}{vN} \quad (28)$$

And the Equ.26 was rewritten as shown below:

$$\sigma = -0.414kT v^{-2/3} \ln(vNc_L) \quad (29)$$

where k is boltzmann constant ($1.38 \times 10^{-23} \text{J K}^{-1}$), T is absolute temperature, v is molecular volume, N is Avogadro constant ($6.02 \times 10^{26} \text{kmol}^{-1}$) and c_L is the solute concentrations (kmol m^{-3}) in the liquid phase.

When the molecular formula of the products is written as $A_1(n_1)A_2(n_2)\dots A_i(n_i)$ (where A_i is atom/molecule and n_i is the number of the A_i atom/molecule), c_L was calculated by the following equation:

$$c_L = \left(\frac{K_{sp}}{n_1^{n_1} \times n_2^{n_2} \times \dots \times n_i^{n_i}} \right)^{\left(\frac{1}{n_1+n_2+\dots+n_i} \right)} \quad (30)$$

According to the previous researches, there has no available data of the v value of the SCHA-A-0.5, SCHA-A-1, SCHA-B-1 and HPO4-SCHA-B-0.5. Thus it was an assumption that the v values of the SCHA-A-0.5, SCHA-A-1, SCHA-B-1 and HPO4-SCHA-B-0.5 are same to that of HA. The values of v and c_L of various apatites were shown in Table 4.

Apatite	$v(m^{-3})$	$c_L(mol/L)$
DCPD	3.09E-28	4.88652 E-04
OCP	3.106E-28	2.28312E-06
DOHA	5.31E-28	8.43452E-07
TCP	1.48E-28	4.82695E-07
HA	5.3E-28	4.09944E-08
SCHA-A-0.5	5.3E-28	3.66998E-08
SCHA-A-1	5.3E-28	1.37127E-06
SCHA-B-1	5.3E-28	4.35071E-06
HPO4-SCHA-B-0.5	5.3E-28	1.96054E-08

Table 4. The values of v and c_L of various apatites

5.2 Calculated results

Fig. 1 shows that the ΔG of various CaPs decrease with increasing the pH (4~10), except of DCPD, of which the ΔG decreased when pH<8 and increased when pH>8 always being higher than zero, agreeing with the previous study [Lu et al., 2005]. At pH=7.4, the ΔG of various CaPs increased as the following sequence: HPO4-SCHA-B-0.5 < SCH A-A-0.5 < HA < TCP < OCP < DOHA < 0 < DCPD < SCH A-A-1 < SCH A-B-1. And the ΔG of HPO4-SCHA-B-0.5 and SCH A-A-0.5 are always lower than that of HA with increasing pH.

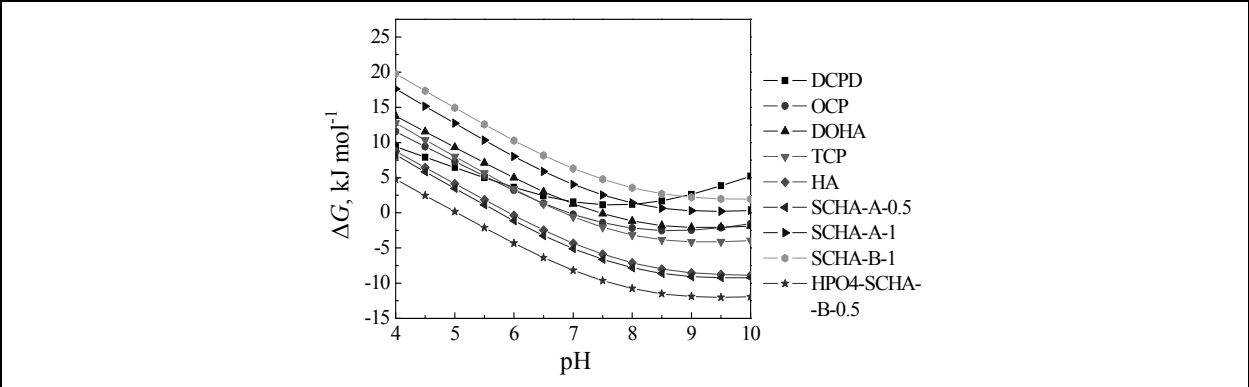


Fig. 1. ΔG for the formation of various CaPs provided by the SBF

This result suggested that the formation of HPO4-SCHA-B-0.5 and SCH A-A-0.5 is thermodynamically easier than the other CaPs. The theoretical calculation results are agreed with the previous experimental result [Weia et al., 2007; Wei et al., 2008]. In Fig. 1, it was also noticed that the ΔG increased obviously when the content of the CO₃²⁻ ions in the CaPs is high by comparison of the ΔG of the HA and SCH A-A-1. Similar result was also observed by comparison of HA and SCH A-B-1.

Fig. 2 shows the change in ΔG with raising the concentrations of Ca²⁺, HPO₄²⁻ and HCO₃⁻ ions and SBF at pH=7.4. The ΔG of various CaPs increased as the following sequence: HPO4-SCHA-B-0.5 < SCH A-A-0.5 < HA < TCP < OCP < DOHA < DCPD < SCH A-A-1 < SCH A-B-1 at different ions concentration. Increasing the concentrations of Ca²⁺ and HPO₄²⁻ ions led to the drop of ΔG of various CaPs as shown Fig. 2a and b, because the augment of Ca²⁺ and HPO₄²⁻ ions concentration improve the lnS of various CaPs according to Eqs.11,12. The increase of the HCO₃⁻ ions seemed to increase the ΔG of various CaPs slightly, as shown in Fig. 2c.

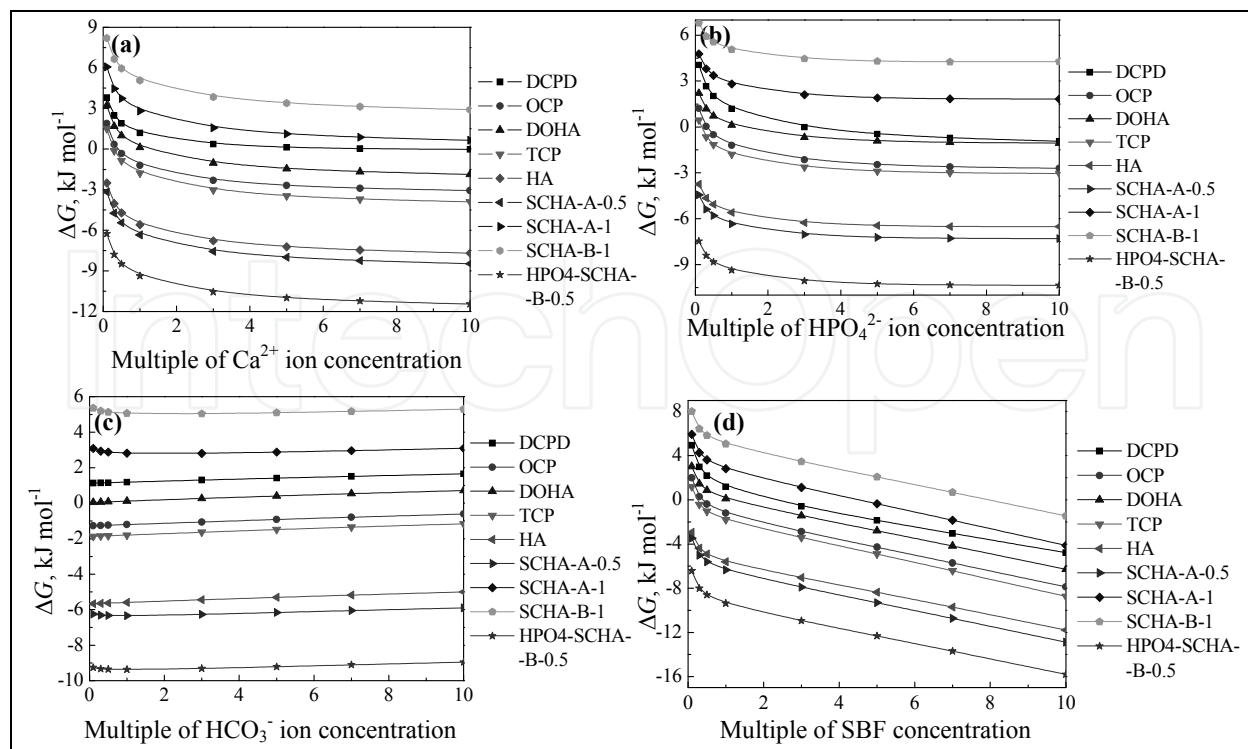


Fig. 2. Change in the ΔG with increasing the multiple of Ca^{2+} , HPO_4^{2-} and HCO_3^- ions concentrations and SBF at pH=7.4: (a) Ca^{2+} , (b) HPO_4^{2-} , (c) HCO_3^- and (d) SBF concentrations.

Fig. 2d shows the decrease in the ΔG with increasing the multiple of SBF concentrations at pH=7.4. The decrease of ΔG is also owing to the increase of $\ln S$ as result of the increase in SBF concentration according to Eqs.11,12. At pH=7.4, the ΔG of the various CaPs always ascend as the following sequence: $\text{HPO4-SCHA-B-0.5} < \text{SCHA-A-0.5} < \text{HA} < \text{TCP} < \text{OCP} < \text{DOHA} < \text{DCPD} < \text{SCHA-A-1} < \text{SCHA-B-1}$ when changing the SBF concentration.

Besides of Ca^{2+} , HPO_4^{2-} and HCO_3^- ions, the effect of other ions in SBF on the ΔG was also taken into account (The figures not shown here). According to the calculated results, when Na^+ ions increased from 0 to 20 multiples, a maximum of the ΔG was observed at the Na^+ ions concentration increasing to about 4 multiples. In the cases of the K^+ and Mg^{2+} ions, the ΔG of the various CaPs increased slightly with increasing concentration. These results suggested that the augment of the K^+ and Mg^{2+} ions is not suitable for the formation of the CaPs, agreeing the previous experimental results [Lu et al., 2005]. The effect of Cl^- ions concentration on the ΔG of various CaPs is similar to that of Na^+ ions. And the effect of SO_4^{2-} ions concentration on the ΔG of various CaPs is not obviously.

Based on the calculation of the S (Eqs. 11,12), the values of the S is greatly dependent on the γ_i corresponding ions in the CaPs, since these CaPs did not contain Na^+ , K^+ , Mg^{2+} , Cl^- and SO_4^{2-} ions. According to the calculated results, it was found that the change of the γ_i is basically contrary with the change of ΔG with increasing the concentrations of Na^+ , K^+ , Mg^{2+} and Cl^- . According to the Eqs. 16 and 17, the γ_i is related with the I . In other words, the change in the concentrations of Na^+ , K^+ , Mg^{2+} , Cl^- and SO_4^{2-} ions could result in the alteration of I , thus eventually, affect the value of γ_i . Based on the Eqs. 11,12, γ_i is larger, and S is higher. Thus the ΔG is lower according to the Equ. 1. In the case of SO_4^{2-} ions, the effect of its concentration on the γ_i is not obvious, thus the ΔG did not alter basically.

Here, two events were also to be noticed. One is that γ_i has a minimum when changing the ions of the SBF. In Equ. 16, it was set that:

$$Y = \frac{I^{1/2}}{1 + I^{1/2}} - 0.3I \quad (31)$$

if γ_i has a minimum, thus the Y should have a maximum with increasing the I . In fact, Y exactly has a maximum based on the calculation of the Equ. 31. When I is at 0.3~0.4, the Y shows a maximum about 0.25.

The other event is that the augment of K⁺ and Mg²⁺ ions concentration led to a very slight increase of ΔG of the various CaPs, unlike changing the Na⁺ and Cl⁻ ions. The reason for this is mainly that the I corresponding to K⁺ and Mg²⁺ ions did not change greatly, because the concentrations of K⁺ and Mg²⁺ ions is greatly lower compared to the Na⁺ and Cl⁻ ions in the SBFs. Thus the slight change in the I , as result of the change of K⁺ and Mg²⁺ ions concentration, is insufficient for alter the Y value. In fact, if the concentrations of K⁺ and Mg²⁺ ions increased to about 1.25 mol/L and 0.3 mol/L, respectively, the ΔG of the various CaPs became to decrease apparently.

Fig. 3 shows that the ΔG of CaPs in the c-SBF, r-SBF, i-SBF and m-SBF are at similar level at pH=7.4; while ΔG of CaPs in HBSS are higher than in the other SBFs. In all SBFs, the CaPs always increased as the following sequence: HPO4-SCHA-B-0.5 < SCHA-A-0.5 < HA < OCP.

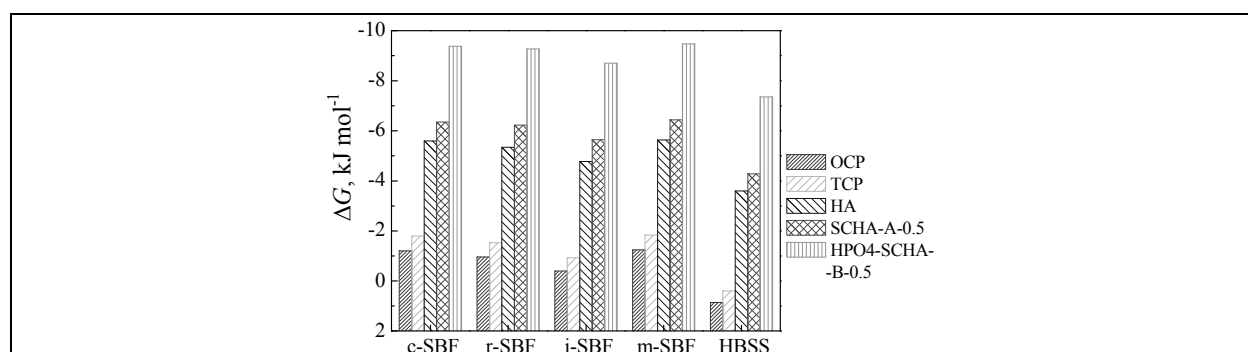


Fig. 3. ΔG for the formation of OCP, HA, SCHA-A-0.5 and HPO4-SCHA-B-0.5 in the different SBFs at pH=7.4.

Fig. 4a shows effect of the pH on the $\log J$ of various CaPs. Because the ΔG of DCPD, SCHA-A-1 and SCHA-B-1 is higher than zero in SBF at pH=7.4, the $\log J$ of these CaPs did not taken into account. The $\log J$ of various CaPs increased as the following sequence: OCP < HA < HPO4-SCHA-B-0.5 < SCHA-A-0.5 at pH=7.4. This result revealed that the formation of SCHA-A-0.5 and HPO4-SCHA-B-0.5 is kinetically favorable. In fact, the previous experimental results also found the trace of A-type substituted carbonated-HA and B-type substituted carbonated-HA containing HPO₄²⁻ group [Müller et al., 2006; Wei^a et al., 2007; Wei et al., 2008].

Totally, the $\log J$ of various CaPs ascended firstly and then descended when increasing pH. And the maximum was observed at pH=9~10, except of OCP, whose maximum occurred at about pH=8.5. When pH<9.5, $\log J$ of HA, HPO4-SCHA-B-0.5 and SCHA-A-0.5 increased as following sequence: HA < HPO4-SCHA-B-0.5 < SCHA-A-0.5. In general, the $\log J$ of the three kinds of CaPs is higher than that of other CaPs.

To understand the effect of various factors on $\log J$, the following Equation was used according to Equ. 22:

$$M = \exp \left(- \frac{16\pi v^2 \sigma^3 f(\theta)}{3k^3 T^3 (\ln S)^2} \right) \quad (32)$$

Thus, the $\log J$ is determined by the P and M based on the Eqs. 22 and 32, neglecting the exact value of K' . Fig. 4b and c shows the effect of the pH on the $\log P$ and $\ln M$ of various CaPs. With increasing the pH, the $\log P$ of TCP, HA, HPO4-SCHA-B-0.5 and SCHA-A-0.5 increased firstly when $\text{pH} < 9 \sim 10$ and then decreased when $\text{pH} > 9 \sim 10$; while that of OCP and DOHA increased slightly. According to Fig. 4c, the $\ln M$ of HA, HPO4-SCHA-B-0.5 and SCHA-A-0.5 did not change with increasing pH; while that of other CaPs increased firstly when $\text{pH} < 9$ and then decreased when $\text{pH} > 9$, especially OCP. These results indicated that the $\log J$ of TCP, is mainly dependent on the $\log P$ when pH was changed; while that of OCP and DOHA is highly determined by the $\ln M$.

From Fig. 4d, the $\ln M$ value changed greatly when $\ln S$ ranged from 0 to 0.5, and did not alter basically when $\ln S > 0.5$. According to the calculated results, the $\ln S$ of HA, HPO4-SCHA-B-0.5 and SCHA-A-0.5 is basically higher than 40 when $\text{pH} > 7$; while that of the OCP and DOHA is just near zero when $\text{pH} > 7$. Thus the $\ln M$ of OCP and DOHA is sensitive to the change of pH according to Fig. 4d.

Fig. 5 shows the change in the $\log J$ with increasing the ions concentrations at $\text{pH} = 7.4$. The $\log J$ of HA and HPO4-SCHA-B-0.5 and SCHA-A-0.5 has a tendency to decrease with increasing Ca^{2+} concentrations; while that of OCP, DOHA and TCP increased, especially OCP as shown in Fig. 5a. However, the $\log J$ of HPO4-SCHA-B-0.5 and SCHA-A-0.5 is always higher than that of other CaPs when Ca^{2+} ions concentration changed in the range of 0~10 multiples. The descent in the $\log J$ of HA and HPO4-SCHA-B-0.5 and SCHA-A-0.5 mainly resulted from the decrease of $\log P$ according to calculated results (not shown here), because the $\ln M$ of these CaPs did not alter basically due to the high $\ln S$ (> 20) compared to OCP, DOHA and TCP. The $\ln S$ of OCP, DOHA and TCP near zero caused a great variety of $\ln M$ value, which further brought out the augment of $\log J$ of these CaPs since the $\log P$ did not alter basically according to calculated results (not shown here).

Fig. 5b shows the change in the $\log J$ with increasing the concentrations of HPO_4^{2-} ions in SBF at $\text{pH} = 7.4$. Except of HPO4-SCHA-B-0.5 showing a tendency to decrease, the $\log J$ of other CaPs mounted up with increasing the concentrations of HPO_4^{2-} ions. And the $\log J$ of SCHA-A-0.5 and HPO4-SCHA-B-0.5 is higher than that of other CaPs when changing concentrations of HPO_4^{2-} ions. According to calculated results (Figures not shown here), the change of $\log P$ of OCP, DOHA and HPO4-SCHA-B-0.5 are similar due to the presence of HPO_4^{2-} ion in their structures and showed a slight decrease. Furthermore, the $\log P$ of other CaPs increased slightly. The effects of the HPO_4^{2-} ions on $\ln M$ and $\ln S$ are similar to those of Ca^{2+} ions. The $\log J$ of OCP, DOHA and TCP is highly dependent on the $\ln M$; while those of HA and SCHA-A-0.5 is mainly determined by the $\log P$.

Fig. 5c shows that the change in the $\log J$ with increasing the concentrations of HCO_3^- ions in SBF at $\text{pH} = 7.4$ is not obviously. Also, the change in the $\log P$, $\ln M$ and $\ln S$ are not evident according to the calculated results (Figures not shown here).

Fig. 5d shows the change in the $\log J$ with increasing the SBF concentrations at $\text{pH} = 7.4$. The $\log J$ of OCP, TCP and DOHA increased and those of other CaPs did not alter basically. Compared to $\log J$, a similar result of the effect of SBF concentrations on $\ln M$ was observed according to the calculated results (not shown here). When the multiple of SBF concentration is larger than four, the $\log J$ of OCP is higher than those of other CaPs. In

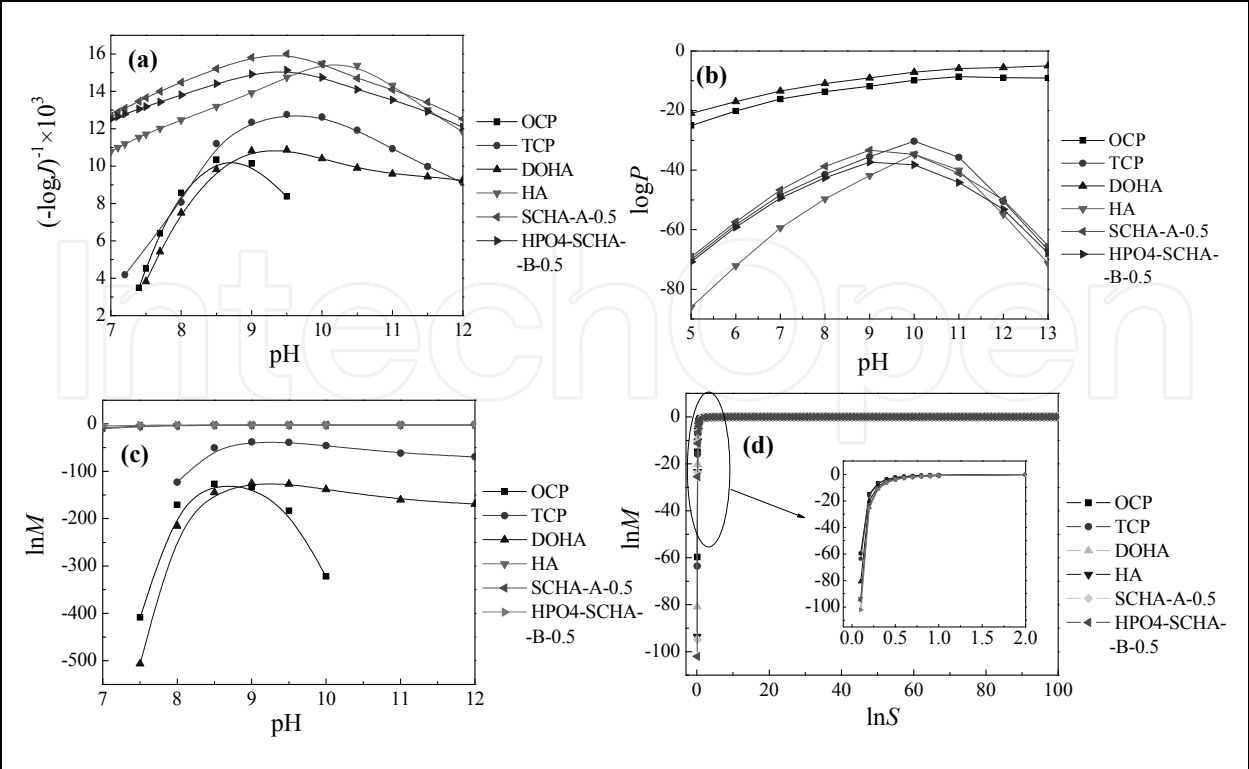


Fig. 4. Effect of pH on the $\log J$, $\log P$ and $\ln M$ of various CaPs with increasing pH: (a) $\log J$, (b) $\log P$, (c) $\ln M$ and (d) the relation between the $\ln S$ and $\ln M$.

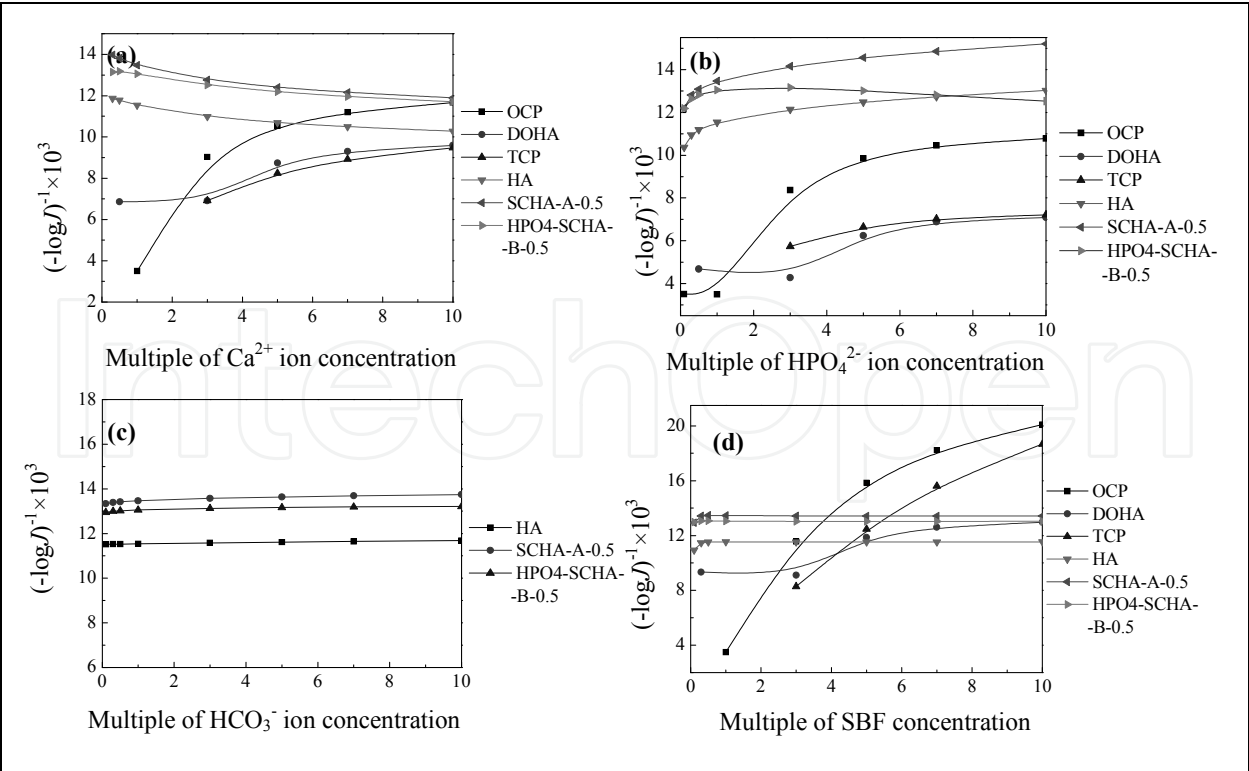


Fig. 5. Change in the $\log J$ with increasing the concentrations of various ions and SBF at pH=7.4: (a) Ca^{2+} , (b) HPO_4^{2-} , (c) HCO_3^- and (d) SBF.

addition, the effect of the SBF concentrations on the $\log P$ is not obvious (not shown here). The calculated results demonstrated that the $\ln S$ of HA, SCH A-A-0.5 and HPO4-SCH A-B-0.5 is higher than 20; while that of OCP, DOHA and TCP varied near the zero, leading to a great variation of $\ln M$.

The effect of Na^+ , K^+ , Mg^{2+} , Cl^- and SO_4^{2-} ions concentration on the $\log J$ of HA, SCH A-A-0.5, SCH A-A-1, SCH A-B-1 and HPO4-SCH A-B-0.5 is not apparent. However, these ions have effect on the $\log J$ of OCP, DOHA and TCP, where the $\log J$ of OCP and TCP decreased firstly, and then increased. And the $\log J$ for DOHA increased with increasing Cl^- ions concentration. With increasing K^+ , Mg^{2+} and SO_4^{2-} ions concentration, the $\log J$ of OCP and TCP lowered slightly.

The $\log J$ of DOHA, OCP and TCP is sensitive for the change of Na^+ and Cl^- ions. The reason for this is that the change of Na^+ and Cl^- ions also has a great effect on the $\ln M$ of the DOHA, OCP and TCP (not shown here). The change in $\ln M$ is associated with the $\ln S$ at here. According to the calculated results, the change of $\ln S$ of DOHA, OCP and TCP nearby the zero, resulting in the great variation in $\ln M$, and $\ln S$ of the other CaPs is greatly higher than zero, which led to an unobvious change in $\ln M$.

Fig. 6 shows the relationships between $\log J$ and v of CaPs. In Fig. 6a, with increasing the v from 200 to 1200 \AA^3 , the $\log J$ of OCP and TCP increased slowly. The change of v did not alter the $\log J$ of other CaPs significantly. At the same time, the $\log J$ increased as the following sequence: $\text{TCP} < \text{OCP} < \text{HA} < \text{HPO4-SCH A-B-0.5} < \text{SCH A-A-0.5}$ as increasing v . This result suggested that the hypothesis of the v of carbonated-HA being equal to that of HA was feasible. In fact, the difference of the v between the carbonated-HA and HA is not significant [Fleet et al., 2004; Kumar et al., 2000]. Further calculating on $\log J$ of CaPs with different v as increasing pH was considered as shown in Fig. 6b. With increasing pH, the change of v did not alter the $\log J$ of HA, HPO4-SCH A-B-0.5 and SCH A-A-0.5. While in the case of OCP, the increase of v improved the $\log J$ slightly.

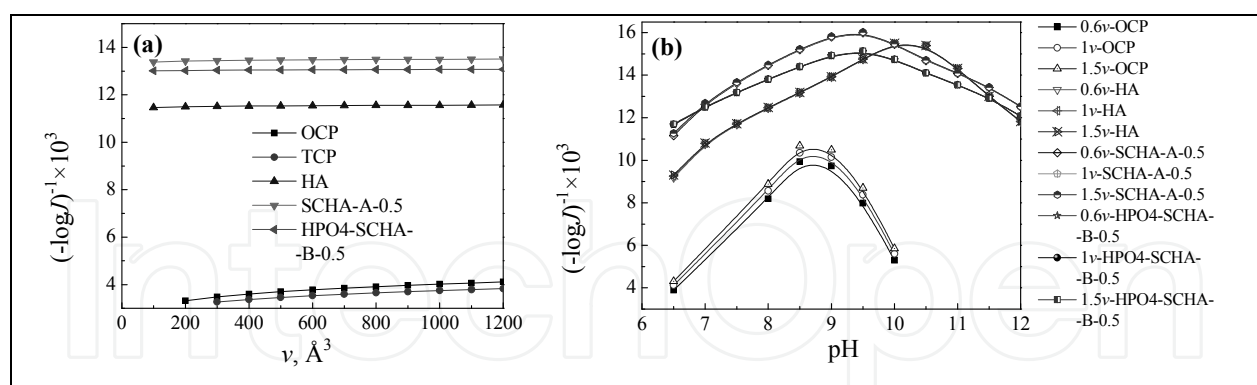


Fig. 6. The relationships between $\log J$ and v of CaPs: (a) change in the $\log J$ with increasing the v of apatites at pH=7.4 and (b) change in the $\log J$ with increasing pH at various v of apatites.

The change in the $\log J$ with increasing the σ at pH=7.4 is shown in Fig. 7a. It was evident that the $\log J$ of the CaPs decreased with increasing the σ , especially of OCP and TCP. The reason for the great decrease in $\log J$ of OCP and TCP is that the change of σ has a great effect on the $\ln M$ as shown in Fig. 7b, which can further influence the $\log J$ of these CaPs. In fact, the previous calculated results also indicated that the effect of σ variation on the $\log J$ was greatly [Lu et al., 2005].

On the other hand, it was difficult to obtain the accurate σ values of the CaPs based on the previous studies [Lu et al., 2005]. Wu and Nancollas summarized the σ of HA, OCP and DCPD acquired by various measurement methods such as contact angle, crystal growth kinetics, dissolution kinetics, etc. [Wu et al., 1999]. Their results showed σ of HA in the range of 9.3~87 mJm⁻², and those of OCP and DCPD in the ranges of 3~45 and 0.4~70 mJm⁻², respectively. In this work, the calculated values of σ are basically in these ranges.

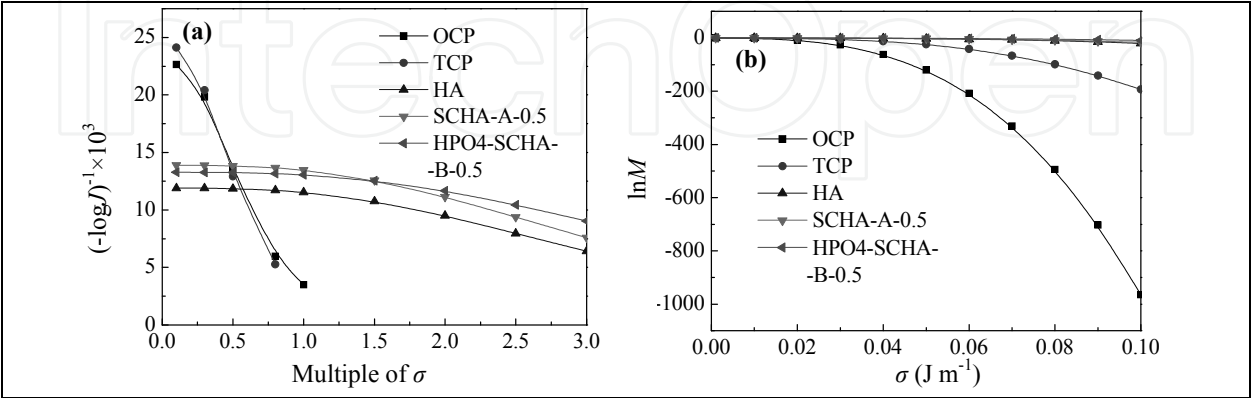


Fig. 7. The relationships between $\log J$ and $\ln M$ and σ of CaPs: (a) change in the $\log J$ with increasing the multiple of σ at pH=7.4 and (b) relation between $\ln M$ and σ at pH=7.4.

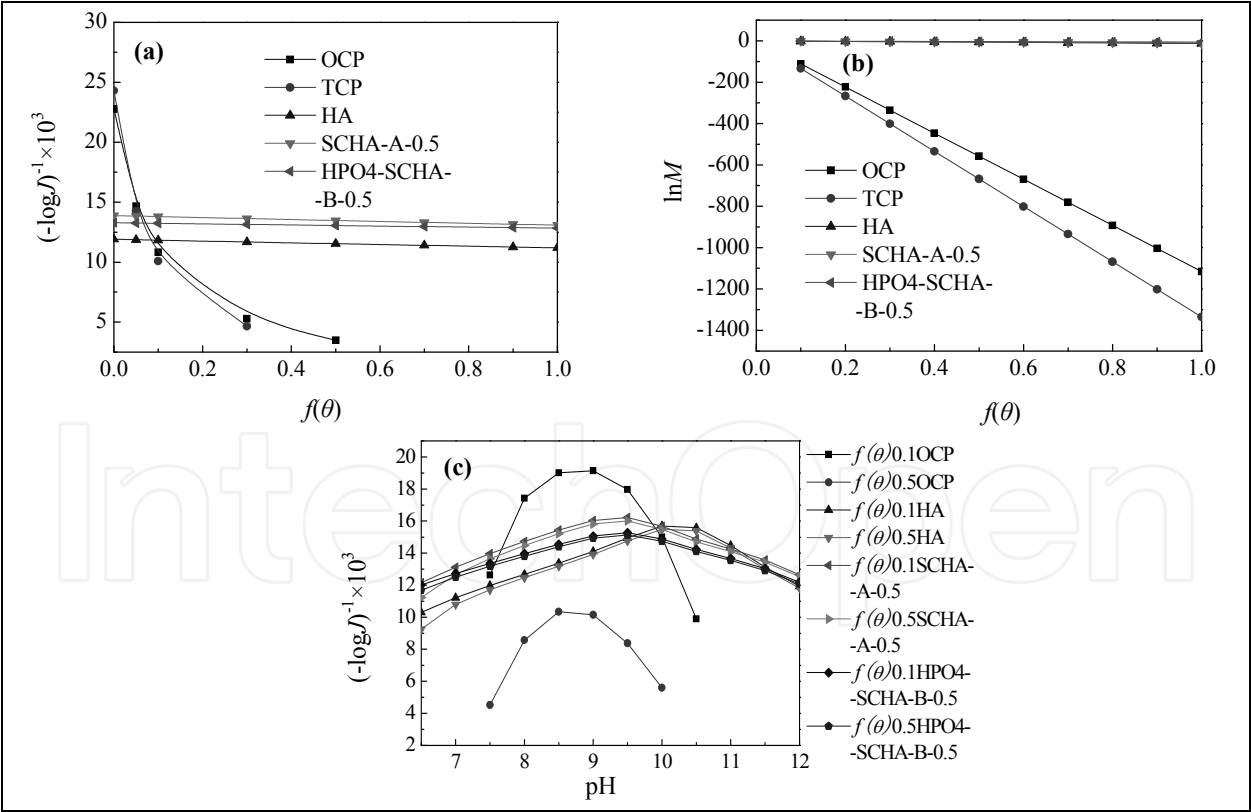


Fig. 8. The relationships among $\log J$, $f(\theta)$, $\ln M$ and pH of CaPs: (a) change in the $\log J$ with increasing the $f(\theta)$ at pH=7.4, (b) relation between $\ln M$ and $f(\theta)$ at pH=7.4 and (c) change in the $\log J$ with increasing pH as using different $f(\theta)$. $f(\theta)0.1$ and $f(\theta)0.5$ means the value of the $f(\theta)$ used at here is 0.1 and 0.5, respectively.

Fig. 8a shows the change in the $\log J$ with increasing $f(\theta)$ at $\text{pH}=7.4$. The $\log J$ of OCP and TCP decreased obviously with increasing $f(\theta)$. However, the $\log J$ of other CaPs did not change basically. The reason for this is that the change of $f(\theta)$ has a great effect on the $\ln M$ of OCP and TCP as shown in Fig. 8b, which can further influence the $\log J$ of these CaPs. The results shown in Fig. 8c indicated that the $\log J$ of OCP is highly dependent on the $f(\theta)$ with increasing pH , and change of $f(\theta)$ has no obvious effects on the $\log J$ of the other CaPs. Fig. 9 shows that the SBFs species did not markedly affect the $\log J$ of HA, SCHA-A-0.5 and HPO4-SCHA-B-0.5 at $\text{pH}=7.4$. Fig. 10a shows the $\log J$ of OCP is highly dependent on the SBF species with increasing pH , and change of SBF species has no obvious effects on the $\log J$ of HA (Fig. 10b).

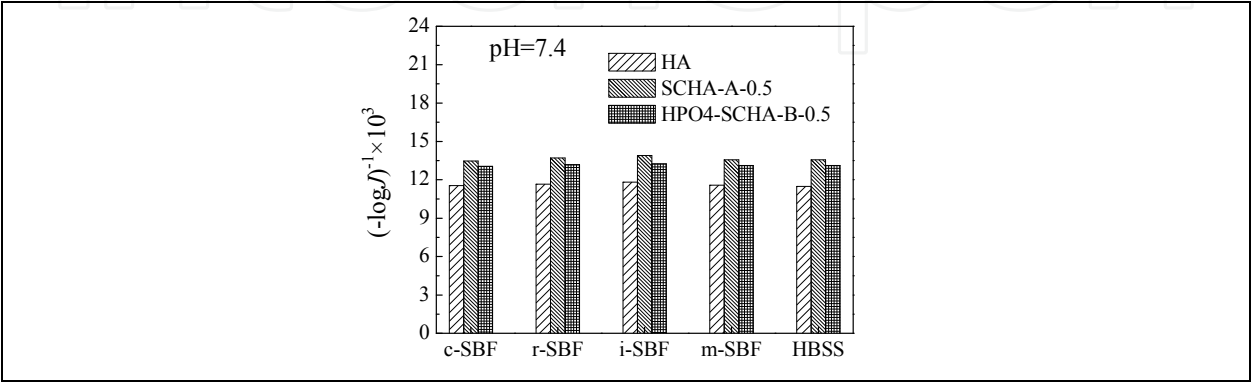


Fig. 9. $\log J$ of HA, SCHA-A-0.5 and HPO4-SCHA-B-0.5 in the different SBFs

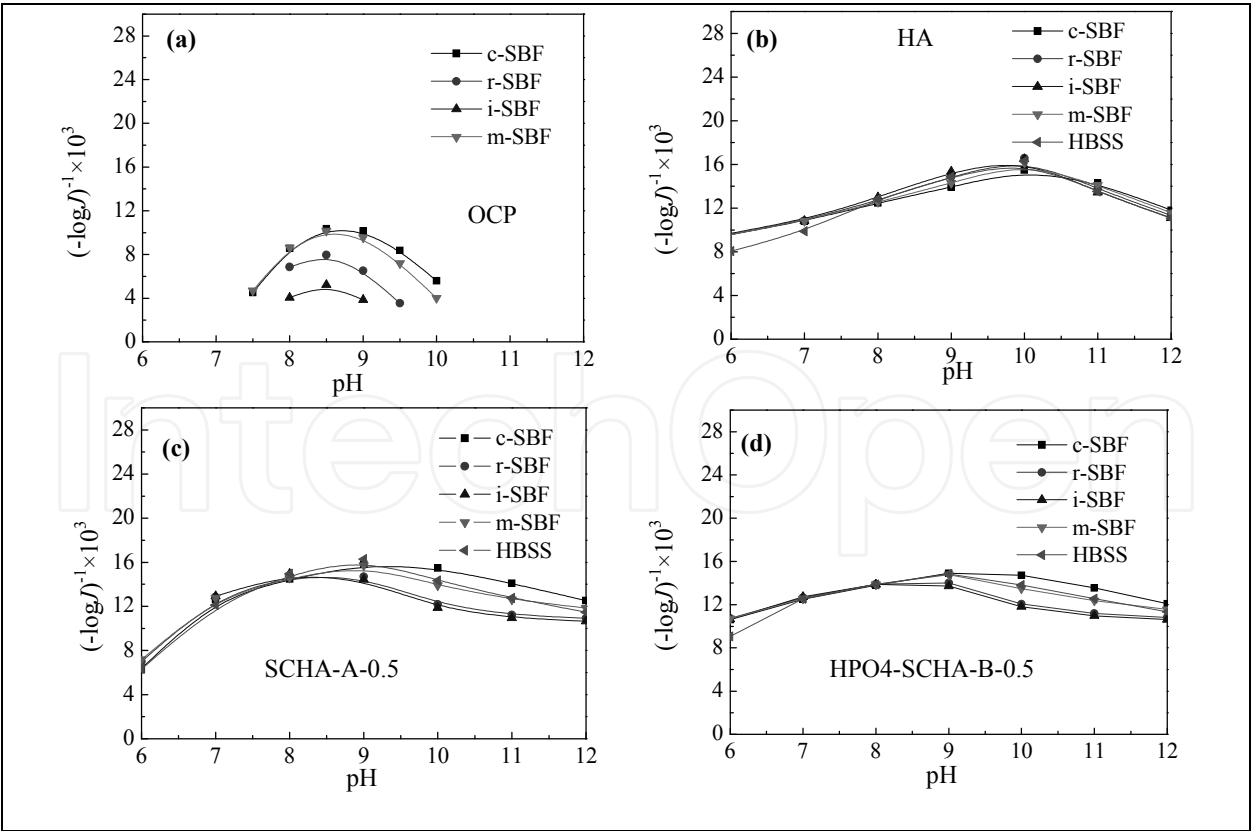


Fig. 10. $\log J$ of various apatites in different SBFs with increasing pH : (a) OCP, (b) HA, (c) SCHA-A-0.5 and (d) HPO4-SCHA-B-0.5.

In the case of OCP, the $\log J$ increased in the four SBFs as the following sequence: i-SBF < r-SBF < m-SBF < c-SBF (Fig. 10a). For SCHA-A-0.5 and HPO₄-SCHA-B-0.5, the effect of SBF species on the $\log J$ is not obvious when pH < 9; while distinction was presented when pH > 9, where the $\log J$ increased as the following sequence: i-SBF \approx r-SBF < m-SBF \approx HBSS < c-SBF (Fig. 10c and d).

In order to understand the change of $\log J$ of OCP, the effect of pH on the $\log P$, $\ln M$ and $\ln S$ were considered. Based on the calculated results, the $\log J$ is mainly determined by the $\ln S$, which determined the change of $\ln M$ here. And the curve of $\ln M$ is similar to the $\log J$ of OCP.

In the case of HA, the pH has no significant effect on $\log P$ and $\ln M$, thus the $\log J$ of HA did not alter obviously.

However the distinguish of $\log J$ of SCHA-A-0.5 and HPO₄-SCHA-B-0.5 in various SBFs appeared when pH > 9. The reason for this is that the change of $\log P$ caused by the SBF species, where the SBF species has no apparent effects on the $\ln M$. The change of $\log P$ is mainly resulted from the different concentrations of HCO₃⁻ ions of SBFs. As shown in the Table 1, the concentrations of HCO₃⁻ ions in various SBFs decreased as following sequence: i-SBF = r-SBF > m-SBF = HBSS > c-SBF, which is just contrary to the change of $\log J$.

5.3 Structure of the bone apatite and biomimetic apatite

As well known, the bones and teeth of all vertebrates are natural composite materials, where one of the components is an inorganic solid, carbonate hydroxyapatite. Thus the formation of the carbonate hydroxyapatite in vitro by biomimetic method is worthy to be noticed. These results indicated whether the induced apatite is A-type or B-type carbonated-HA, the high concentration of CO₃²⁻ ions in carbonated-HA deter its formation. In other words, the dissolution of highly carbonated-HA could be serious relatively. In fact, the previous results indicated that CO₃²⁻ ions concentration in carbonated-HA is higher, the dissolving of carbonated HA is faster [Okazaki, et al., 1999].

Besides CO₃²⁻ ions, HPO₄²⁻ ions also is one component of the bone apatite. The carbonated-HA of bones ranges between 4% and 8% in carbonate content, which increases with age while HPO₄²⁻ ions decreases. In this work, the theoretical calculation results indicated that the introduction of HPO₄²⁻ ions lowered the ΔG of carbonated HA. In fact, biomimetic apatite containing HPO₄²⁻ ions have been reported.

Also, Na⁺, K⁺, Mg²⁺ and Cl⁻ ions can incorporate the structure of apatite. Thus, the chemical composition of apatite could be more complex. If Na⁺, K⁺, Mg²⁺ and Cl⁻ ions were considered, more equations regarding to calculating their equilibrium concentrations were needed. Thus mathematic method and computer language are needed to solve the high order equation such as quintic equation. In addition, no details parameters of these CaPs in the thermodynamic and kinetic calculations such as K_{sp} , v , σ , $f(\theta)$ etc. can be available. According to these, it was difficult to conduct the thermodynamic and kinetic calculations of apatite formation when the chemical compositions of apatite become more abundant.

5.4 Nuclear and growth

Due to SBF with high concentration, the apatite body was formed at the early stage of the SBF immersion process as shown Fig. 11a. With increasing the SBF immersion time, the apatite body grew, resulting in a decrease in SBF concentration (red line). When the size of apatite body reached r_c , and the SBF concentration is higher than c_c . Thus the apatite nuclear

was formed, which could further grow due to the high concentration of SBF. And the SBF concentration continuously decreased due to the growth of the apatite nuclear. When the SBF concentration reached an equilibrium concentration, the sized of the apatite particle did not increase.

During total process of apatite formation, the apatite grew by consuming calcium ions and phosphate radicals, et al.. At the same time, the apatite could was dissolved, releasing calcium ions and phosphate radicals, et al.. When SBF concentration is higher than equilibrium concentration, the deposition rate of apatite is greater than dissolution rate of apatite. When SBF concentration is equal to equilibrium concentration, the deposition rate of apatite is equal to the dissolution rate of apatite.

If the initial concentration of SBF is lower than c_c , thus the apatite nuclear can not be formed. Even if the apatite body (its size less than r_c) was formed, it usually disappeared due to no superfluous ions to supply the deposition of apatite body. Thus, the apatite formation is highly dependent on the ions concentration near the surface of bioactive coatings based on the above discussion. Just the attraction of functionalized surfaces for other ions caused the increase in ions concentration near the local surface. Based on the above equation, the r_c of CaPs was calculated. It was observed that the r_c decreased as the following sequence: OCP > TCP >> HA > SCH A-A-0.5 > HPO4-SCHA-B-0.5. These results suggested that the formation of SCH A-A-0.5 and HPO4-SCHA-B-0.5 is easier compared with other CaPs.

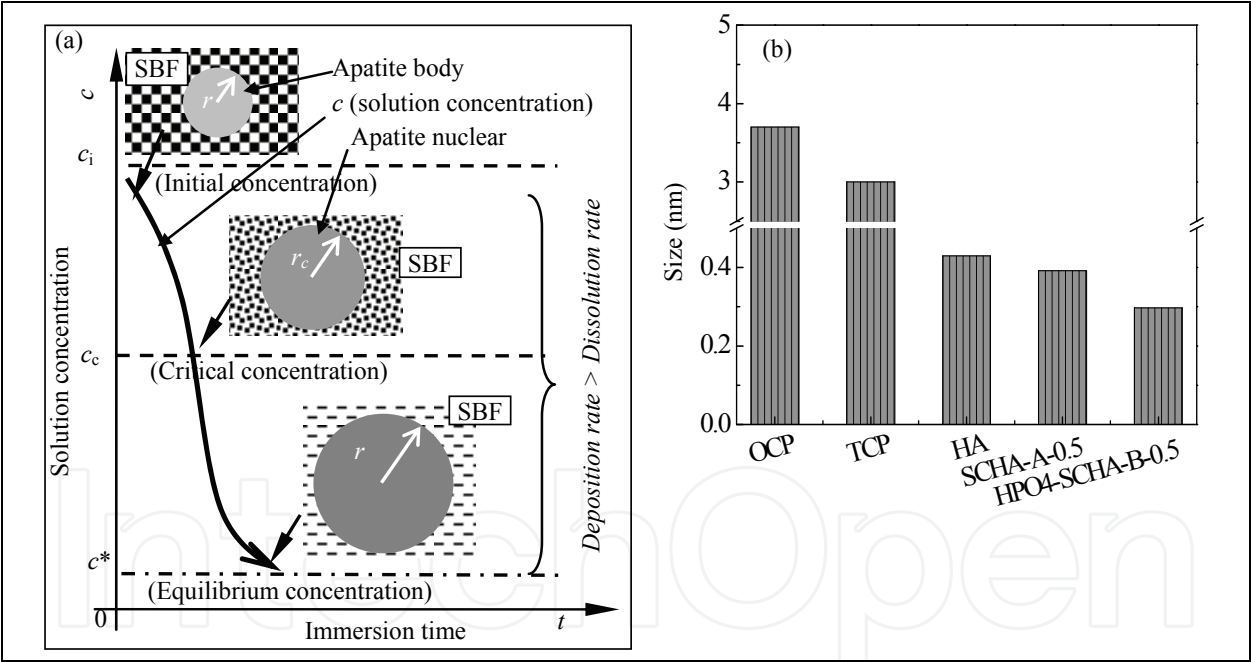


Fig. 11. Nuclear and growth of apatites in SBF: (a) schametical diagram for the formation and growth of apatite nuclear during the SBF immersion process and (b) r_c of various CaPs nuclear in the SBF.

5.5 Phase transformation of biomimetic apatite

The previous results indicated that the gel-like matter was formed on the surface of the chemical-treated MAO coatings at the early stage of the SBF immersion process. The gel-like matter mainly contained Ca and P elements with an amorphous structure. After further immersion, the amorphous Ca and P could transform to crystal phase.

In fact, the formation of apatite on the surface of substrates is a very complex process, since various factors have effect on the apatite nucleation and growth such as supersaturation or the solution compositions, interface energy and contacting angle of apatites and substrates, etc..

The precipitation of apatite from SBF or the supersaturated calcium phosphate solution (differing from SBF in composition containing higher Ca and P concentrations) has been widely investigated in the past [Feng et al., 1999; Li et al., 2002; Barrère et al., 1999; Lu et al., 2004; Lu et al., 2007; Horváthová et al., 2008; Xie et al., 2006]. Experimental observation indicated that some important characteristics of the initial behaviors of apatite formation. Feng et al. [Feng et al., 1999; Li et al., 2002] observed various apatites such as DCPD, OCP and HA phases on the surfaces of alkali-treated titanium when the samples were immersed in supersaturated calcification solution. Leng [Lu et al., 2004] used transmission electron microscopy (TEM) to investigate the formation of calcium phosphate on alkali- and heat-treated titanium surfaces in a revised SBF. In their results, electron diffraction of the precipitates revealed that OCP, instead of HA, directly nucleates from amorphous CaP. The OCP crystals continuously grew on the titanium surfaces rather than transforming into apatite. Lu et al. [Lu et al., 2007] found that amorphous CaP coatings were formed on the surfaces by immersing the nitric acid treated Ti specimens in SBF, while OCP coatings were formed in the supersaturated calcium phosphate solution after 3 days of immersion. And, OCP could further transfer into carbonated-HA in SBF [Horváthová et al., 2008].

Based on the this investigation, compared to HA and carbonated-HA, the formation of OCP is highly dependent on $f(\theta)$, σ and local ions concentration near substrate surfaces. This probably is the main reason for forming OCP and sometimes not during the immersion process in Ca- and P-containing solutions. In other words, OCP is not the necessary intermediate phase for the formation of HA or carbonated-HA, and the formation of OCP is associated with the circumstance, especially the contacting angle between OCP and substrate and local ions concentration.

6. Conclusion

MAO is a relatively convenient and effective technique to deposit bioceramic coatings on the surfaces of Ti and its alloys. The structures such as phase composition, surface morphology and elemental composition of the MAO coatings are highly dependent on the applied voltage, oxidizing time, frequency, duty cycle and electrolyte composition, etc., especially the applied voltage and electrolyte composition.

The apatite-forming ability and bioactivity of most of MAO coatings are not very good. Thus, subsequent activation methods such as sol-gel, UV irradiation and hydrothermal treatments have been investigated to improve the surface bioactivity of MAO coatings. Authors have developed a simple chemical-treatment to modify the surface of the MAO coatings. A variety of reactions such as dissolution, ion exchange and precipitation took place on the surface of the chemical-treated MAO coating during the SBF immersion process to form Ti-OH groups, which greatly improved the apatite-forming ability of the MAO coatings.

The induced biomimetic apatites were SCHA-A and HPO₄-SCHA-B. At the same time, Na, K, Mg and Cl elements could be also introduced into these apatites, however, the concentrations of these elements are very small. In addition, the induced biomimetic apatite presented two-level porous structure on micro- and nano-scales.

The theoretical calculated result indicated that the formation of A-type slightly substituted carbonated-HA and B-type slightly substituted carbonated-HA containing HPO_4^{2-} ions is thermodynamically and kinetically easier than other CaPs, consistent with the experimental results. The pH, ions concentrations and species of SBFs greatly affected the ΔG and $\log J$ of CaPs. Totally, the ΔG of CaPs descend with increasing pH and concentration multiple of SBF and Ca^{2+} and HPO_4^{2-} ions concentrations. Moreover, other factors such as surface tension, contacting angle and molecular volume can affect the $\log J$ of CaPs, especially $\text{Ca}_4(\text{HPO}_4)(\text{PO}_4)_2$, $\text{Ca}_3(\text{PO}_4)_2$ and $\text{Ca}_9(\text{HPO}_4)(\text{PO}_4)_5\text{OH}$.

The surface topography, surface energy and wetting properties etc. are important factors to affect the osteoblast adhesion and proliferation. The current results indicated that MAO coatings and modified MAO coatings show good biocompatibility according to the cell proliferation tests in vitro.

7. References

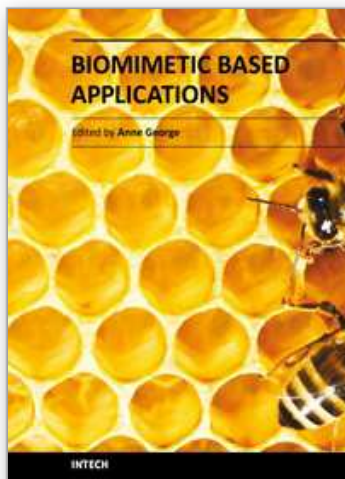
- Balamurugan, A.; Balossier, G.; Kannan, S.; Michel, J.; Rebelo, A.H.S. & Ferreira, J.M.F. (2007). Development and in vitro characterization of sol-gel derived $\text{CaO-P}_2\text{O}_5\text{-SiO}_2\text{-ZnO}$ bioglass. *Acta Biomater*, Vol. 3, No. 2, March 2007, 255-262, ISSN: 1742-7061
- Barrère, F.; Layrolle, P.; Blitterswijk, C.A.V. & Groot, K.D. (1999). Biomimetic calcium phosphate coatings on Ti6Al4V: a crystal growth study of octacalcium phosphate and inhibition by Mg^{2+} and HCO_3^{2-} . *Bone*, Vol. 25, No. 2, Supplement 1, August 1999, 107S-111S, ISSN: 8756-3282
- Boistelle, R. & Lopez-valero, I. (1990). Growth units and nucleation: the case of calcium phosphates. *J of Crystal Growth*, Vol. 102, No. 3, May 1990, 609-617, ISSN: 0022-0248
- Feng, Q.L.; Wang, H.; Cui, F.Z. & Kim, T.N. (1999). Controlled crystal growth of calcium phosphate on titanium surface by NaOH-treatment. *Journal of Crystal Growth*, Vol. 200, No. 3-4, April 1999, 550-557, ISSN: 0022-0248
- Feng, Q.L.; Cui, F.Z.; Wang, H.; Kim, T.N. & Kim, J.O. (2000). Influence of solution conditions on deposition of calcium phosphate on titanium by NaOH-treatment. *Journal of Crystal Growth*, Vol. 210, No. 4, March 2000, 735-740, ISSN: 0022-0248
- Fini, M.; Cigada, A. & Rondelli, G. (1999). In vitro and in vivo behaviour of Ca- and P-enriched anodized titanium. *Biomaterials*, Vol. 20, No. 17, September 1999, 1587-1594, ISSN: 0142-9612
- Fleet, M.E. & Liu, X.Y. (2004). Location of type B carbonate ion in type A-B carbonate apatite synthesized at high pressure. *Journal of Solid State Chemistry*, Vol. 177, No. 9, September 2004, 3174-3182, ISSN: 0022-4596
- Frauchiger, V.M.; Schlottig, F.; Gasser, B. & Textor, M. (2004). Anodic plasma-chemical treatment of CP titanium surfaces for biomedical applications. *Biomaterials*, Vol. 25, No. 4, February 2004, 593-606, ISSN: 0142-9612
- Han, Y.; Hong, S.H. & Xu, K.W. (2003). Structure and in vitro bioactivity of titania-based films by micro-arc oxidation. *Surf Coat Technol.*, Vol. 168, No. 2-3, 22 May 2003, 249-258, ISSN: 0257-8972

- Han, Y.; Chen, D.H.; Sun, J.F.; Zhang, Y.M. & Xu, K.W. (2008). UV-enhanced bioactivity and cell response of micro-arc oxidized titania coatings. *Acta Biomaterialia*, Vol. 4, No. 5, September 2008, 1518-1529, ISSN: 1742-7061
- Heughebaert, J.C^a. & Nancollas, G.H. (1984). Kinetics of crystallization of octacalcium phosphate. *J Phys Chem*, June 1984, 88 (12), 2478-2481.
- Heughebaert, J.C^b. & Nancollas, G.H. (1984). Mineralization kinetics—the role of octacalcium phosphate in the precipitation of calcium phosphates. *Colloid Surf*, Vol. 9, No. 1, 1 March 1984, 89-93.
- Horváthová, Renáta.; Müller, Lenka.; Helebrant, A.; Greil, P. & Müller, F.A. (2008). In vitro transformation of OCP into carbonated HA under physiological conditions. *Materials Science and Engineering C*, Vol. 28, No. 8, December 2008, 1414-1419, ISSN: 0928-4931
- Huang, P.; Zhang, Y.; Xu, K.W. & Han, Yong. (2004). Surface modification of titanium implant by microarc oxidation and hydrothermal treatment. *J Biomed Mater Res Part B: Appl Biomater* 70B: Vol. 70B, No. 2, 15 August 2004, 187-190, ISSN: 0021-9304
- Ishizawa, H. & Ogino, M. (1995). Characterization of thin hydroxyapatite layers formed on anodic titanium oxide coatings containing Ca and P by hydrothermal treatment. *Journal of Biomedical Materials Research*, Vol. 29, No. 9, September 1995, 1071-1079, ISSN: 0021-9304
- Koutsopoulos, S.; Paschalakis, P.C. & Dalas, E. (1994). The calcification of elastin in vitro. *Langmuir*, Vol. 10, No. 7, July 1994, 2423-2428, ISSN: 0743-746
- Koutsopoulos, S. & Dalas, E. (2000). The calcification of fibrin in vitro. *J Cryst Growth*, Vol. 216, No. 1-4, 15 June 2000, 450-458, ISSN: 0022-0248
- Koutsoukos, P.G.; Amjad, Z.; Tomson, M.B. & Nancollas, G.H. (1980). Crystallization of calcium phosphates—a constant composition study. *J Am Chem Soc*, Vol. 102, No. 5, February 1980, 1553-1557
- Koutsoukos, P.G. & Nancollas, G.H. (1981). Crystal growth of calcium phosphates—epitaxial considerations. *J Cryst Growth* Vol. 53, No. 1, May 1981, 10-19
- Kumar, T.S.S.; Manjubala, I. & Gunasekaran, J. (2000). Synthesis of carbonated calcium phosphate ceramics using microwave irradiation. *Biomaterials*, Vol. 21, No. 16, August 2000, 1623-1629, ISSN: 0142-9612
- Li, F.; Feng, Q.L.; Cui, F.Z.; Li, H.D. & Schubert, H. (2002). A simple biomimetic method for calcium phosphate coating. *Surface and Coatings Technology*, Vol. 154, No. 1, May 2002, 88-93, ISSN: 0257-8972
- Li, L.H.; Kong, Y.M. & Kim, H.W. (2004). Improved biological performance of Ti implants due to surface modification by micro-arc oxidation. *Biomaterials*. Vol. 25, No. 14, June 2004, 2867-2875, ISSN: 0142-9612
- Li, L.H.; Kim H.W.; Lee, S.H.; Kong, Y.M. & Kim, H.E. (2005). Biocompatibility of titanium implants modified by microarc oxidation and hydroxyapatite coating. Wiley Periodicals, Inc. *J Biomed Mater Res A*, Vol. 73, No. 1, April 2005, 48-54, ISSN: 1549-3296
- Liu, Q.; Ding, J.; Mante, F.K.; Wunde, S.L. & Baran, G.R. (2002). The role of surface functional groups in calcium phosphate nucleation on titanium foil: a self-

- assembled monolayer technique. *Biomaterials*, Vol. 23, No. 15, August 2002, 3103-3111, ISSN: 0142-9612
- Liu, X.Y.; Paul, K.C. & Ding, C.X. (2004). Surface modification of titanium, titanium alloys, and related materials for biomedical applications. *Mater Sci Eng R*, Vol. 47, No. 3-4, December 2004, 49-121, ISSN: 0927-796X
- Lu, X. & Leng, Y. (2004). TEM study of calcium phosphate precipitation on bioactive titanium surfaces. *Biomaterials*, Vol. 25, No. 10, May 2004, 1779-1786, ISSN: 0142-9612
- Lu, X.; Zhao, Z.F. & Leng, Yang. (2007). Biomimetic calcium phosphate coatings on nitric-acid-treated titanium surfaces. *Materials Science and Engineering C*, Vol. 27, No. 4, May 2007, 700-708, ISSN: 0928-4931
- Morais, L.S.; Serra, G.G.; Muller, C.A.; Andrade, L.R.; Palermo, E.F.A.; Elias, C.N. & Meyers, M. (2007). Titanium alloy mini-implants for orthodontic anchorage: Immediate loading and metal ion release. *Acta Biomater*, Vol. 3, No. 3, May 2007, 331-339, ISSN: 1742-7061
- Müller, L. & Müller, F.A. (2006). Preparation of SBF with different HCO_3^- content and its influence on the composition of biomimetic apatites. *Acta Biomater*, Vol. 2, No. 2, March 2006, 181-189, ISSN: 1742-7061
- Mullin, J.W. (2001). Crystallization. Butterworth-Heinemann. UK :86-214
- Okazaki, M. & Takahashi, J. (1999). Synthesis of functionally graded CO_3 apatite as surface biodegradable crystals. *Biomaterials*, Vol. 20, No. 12, June 1999, 1073-1078 ISSN: 0142-9612
- Oyane, A.; Kim, H.M.; Furuya, T.; Kokubo, T.; Miyazaki, T. & Nakamura, T. (2003). Preparation and assessment of revised simulated body fluids. *J Biomed Mater Res A*, Vol. 65A, No. 2, 188-195, 1 May 2003 ISSN: 0021-9304
- Rodriguez, R.; Kim, K.H. & Ong, J.L. (2003). In vitro osteoblast response to anodized titanium and anodized titanium followed by hydrothermal treatment. *J Biomed Mater Res A*, Vol. 65, No. 3, June 2003, 352-358, ISSN: 0021-9304
- Song, W.H.; Jun, Y.K.; Han, Y. & Hong, S.H. (2004). Biomimetic apatite coatings on microarc oxidized titania. *Biomaterials*, Vol. 25, No. 17, August 2004, 3341-3349, ISSN: 0142-9612
- Song, W.H.; Ryu, H.S. & Hong, S.H. (2005). Apatite induction on Ca-containing titania formed by micro-arc oxidation. *J Am Ceram Soc*, Vol. 88, No. 9, September 2005, 2642-2644, ISSN: 0002-7820
- Toworfe, G.K.; Composto, R.J.; Shapiro, I.M. & Ducheyne, P. (2006). Nucleation and growth of calcium phosphate on amine-, carboxyl- and hydroxyl-silane self-assembled monolayers. *Biomaterials*, Vol. 27, No. 4, February 2006, 631-642, ISSN: 0142-9612
- Wang, Y.M.; Guo, L.X.; Ouyang, J.H.; Zhou, Y. & Jia, D.C. (2009). Interface adhesion properties of functional coatings on titanium alloy formed by microarc oxidation method. *Applied Surface Science*, Vol. 255, No. 15, May 2009, 6875-6880, ISSN: 0169-4332
- Wei, D.Q.^a; Zhou, Y.; Jia, D.C. & Wang, Y.M. (2007). Characteristic and in vitro bioactivity of microarc oxidized TiO_2 -based coating after chemical treatment. *Acta Biomater*, Vol. 3, No. 5, September 2007, 817-827, ISSN: 1742-7061

- Wei, D.Q^b.; Zhou, Y.; Jia, D.C. & Wang, Y.M. (2007). Effect of applied voltage on the structure of microarc oxidized TiO₂-based bioceramic films. *Mater. Chem. Phys.*, Vol. 104, No. 1, July 2007, 177-182, ISSN: 0254-0584
- Wei, D.Q^c.; Zhou Y.; Wang Y.M. & Jia D.C. (2007). Characteristic of microarc oxidized coatings on titanium alloy formed in electrolytes containing chelate complex and nano-HA. *Appl. Surf. Sci.*, Vol. 253, No. 11, March 2007, 5045-5050, ISSN: 0169-4332
- Wei, D.Q.; Zhou, Y.; Wang, Y.M. & Jia, D.C. (2008). Chemical etching of micro-plasma oxidized titania film on titanium alloy and apatite deposited on the surface of modified titania film in vitro. *Thin Solid Films*, Vol. 516, No. 8, February 2008, 1818-1825, ISSN: 0040-6090
- Wei, D.Q.; Zhou, Y. & Yang, C.H. (2009). Structure, cell response and biomimetic apatite induction of gradient TiO₂-based/nano-scale hydrophilic amorphous titanium oxide containing Ca composite coatings before and after crystallization. *Colloids and Surfaces B: Biointerfaces*, Vol. 74, No. 1, November 2009, 230-237, ISSN: 0927-7765
- Wen, C.E.; Xu, W.; Hu, W.Y. & Hodgson, P.D. (2007). Hydroxyapatite/titania sol-gel coatings on titanium-zirconium alloy for biomedical applications. *Acta Biomater*, Vol. 3, No. 3, May 2007, 403-410, ISSN: 1742-7061
- Wu, W. & Nancollas, G.H. (1997). Nucleation and crystal growth of octacalcium phosphate on titanium oxide surfaces. *Langmuir*, Vol. 13, No. 4, February 1997, 861-865, ISSN: 0743-7463
- Wu, W. & Nancollas, G.H. (1999). Determination of interfacial tension from crystallization and dissolution data: a comparison with other methods. *Adv Colloid Interface Sci*, Vol. 79, No. 2-3, February 1999, 229-279, ISSN: 0001-8686
- Xie, Y.T.; Liu, X.Y.; Chu, P.K. & Ding, C.X. (2006). Nucleation and growth of calcium-phosphate on Ca-implanted titanium surface. *Surface Science*, Vol. 600, No. 3, February 2006, 651-656, ISSN: 0039-6028
- Xiong, Lu. & Yang, Leng. (2005). Theoretical analysis of calcium phosphate precipitation in simulated body fluid. *Biomaterials*, Vol. 26, No. 10, April 2005, 1097-1108, ISSN: 0142-9612
- Yerokhin, A.L.; Nie, X.; Leyland, A.; Matthews, A. & Dowey, S.J. (1999). Plasma electrolysis for surface engineering. *Surf Coat Technol*, Vol. 122, No. 2-3, December 1999, 73-93, ISSN: 0257-8972
- Zhang, Q.Y.; Leng, Y. & Xin, R.L. (2005). A comparative study of electrochemical deposition and biomimetic deposition of calcium phosphate on porous titanium. *Biomaterials*, Vol. 26, No. 16, June 2005, 2857-2865, ISSN: 0142-9612
- Zhang, Y.M.; Bataillon-Linez, P.; Huang, P.; Zhao, Y.M.; Han, Y.; Traisnel, M.; Xu, K.W. & Hildebrand, H.F. (2004). Surface analyses of micro-arc oxidized and hydrothermally treated titanium and effect on osteoblast behavior. *J Biomed Mater Res A*, Vol. 68A, No. 2, February 2004, 383-391, ISSN: 0021-9304
- Zheng, X.B.; Huang, M.H. & Ding, C.X. (2000). Bond strength of plasma-sprayed hydroxyapatite/Ti composite coatings. *Biomaterials*, Vol. 21, No. 8, April 2000, 841-849, ISSN: 0142-9612

- Zhu, X.L.; Kim, K.H. & Jeong, Y.S. (2001). Anodic oxide films containing Ca and P of titanium biomaterial. *Biomaterials*, Vol. 22, No. 16, August 2001, 2199-2206, ISSN: 0142-9612
- Zhu, X.L.; Ong, J.L.; Kim, S.Y. & Kim, K.H. (2002). Surface characteristics and structure of anodic oxide films containing Ca and P on a titanium implant material. *J Biomed Mater Res*, Vol. 60, No. 2, May 2002, 333-338, ISSN: 0021-9304



Biomimetic Based Applications

Edited by Prof. Marko Cavrak

ISBN 978-953-307-195-4

Hard cover, 572 pages

Publisher InTech

Published online 26, April, 2011

Published in print edition April, 2011

The interaction between cells, tissues and biomaterial surfaces are the highlights of the book "Biomimetic Based Applications". In this regard the effect of nanostructures and nanotopographies and their effect on the development of a new generation of biomaterials including advanced multifunctional scaffolds for tissue engineering are discussed. The 2 volumes contain articles that cover a wide spectrum of subject matter such as different aspects of the development of scaffolds and coatings with enhanced performance and bioactivity, including investigations of material surface-cell interactions.

How to reference

In order to correctly reference this scholarly work, feel free to copy and paste the following:

Daqing Wei and Yu Zhou (2011). Bioactive Microarc Oxidized TiO₂-based Coatings for Biomedical Implication, Biomimetic Based Applications, Prof. Marko Cavrak (Ed.), ISBN: 978-953-307-195-4, InTech, Available from: <http://www.intechopen.com/books/biomimetic-based-applications/bioactive-microarc-oxidized-tio2-based-coatings-for-biomedical-implication>

INTech
open science | open minds

InTech Europe

University Campus STeP Ri
Slavka Krautzeka 83/A
51000 Rijeka, Croatia
Phone: +385 (51) 770 447
Fax: +385 (51) 686 166
www.intechopen.com

InTech China

Unit 405, Office Block, Hotel Equatorial Shanghai
No.65, Yan An Road (West), Shanghai, 200040, China
中国上海市延安西路65号上海国际贵都大饭店办公楼405单元
Phone: +86-21-62489820
Fax: +86-21-62489821

© 2011 The Author(s). Licensee IntechOpen. This chapter is distributed under the terms of the [Creative Commons Attribution-NonCommercial-ShareAlike-3.0 License](https://creativecommons.org/licenses/by-nc-sa/3.0/), which permits use, distribution and reproduction for non-commercial purposes, provided the original is properly cited and derivative works building on this content are distributed under the same license.

IntechOpen

IntechOpen